A COMPUTATIONAL FLUID DYNAMIC APPROACH AND MONTE CARLO SIMULATION OF PHANTOM MIXING TECHNIQUES FOR QUALITY CONTROL TESTING OF GAMMA CAMERAS

A thesis submitted in partial fulfilment of the requirements for the

Degree of Master of Science in Medical Physics

in the University of Canterbury

By

Qing YANG

University of Canterbury

2013

Table of contents

List of Figures

List of Tables

Acknowledgments

Firstly, I wish to express my appreciation to my supervisors Dr Darin O'Keeffe and Dr Juergen Meyer for their time, patience and support to this project. Secondly, I would like to thank Dr Mike Reid and Prof Catherine Moran for their understanding and help. Finally, I would also like to thank my father Yanlong Yang, my mother Xiaolin She, my wife Yang Zhao, my mother in law Lihua Han and my father in law Qinlu Zhao for the support they provided me through my entire life. I could not finish this thesis without the love of yours.

Abbreviations

ALARA.	As Low as Reasonably Achievable
CFD	Computational Fluid Dynamics
Co57.	A radioactive form of the element cobalt
CPS	Count per second
DICOM	Digital Imaging and Communications in Medicine
FWHM	Full Width at Half Maximum
keV	kiloelectron Volt (1000 electron Volts)
LEHR.	Low Energy High Resolution
LSF	Line Spread Function
MBq.	Megabecquerel (1 million counts per second)
MC	Monte Carlo
Mo-99	Molybdenum-99. The parent nuclide of Tc-99m
MRI.	Magnetic Resonance Imaging
QC	Quality Control
PET.	Positron Emission Tomography
SPECT.	Single Photon Emission Tomography
Tc99m	The isomeric state of Tc99m
UDF	User Defined Fuction

Abstract

In order to reduce the unnecessary radiation exposure for the clinical personnel, the optimization of procedures in the quality control test of gamma camera was investigated. A significant component of the radiation dose in performing the quality control testing is handling phantoms of radioactivity, especially the mixing to get a uniform activity concentration. Improving the phantom mixing techniques appeared to be a means of reducing radiation dose to personnel. However, this is difficult to perform without a continuous dynamic tomographic acquisition system to study mixing the phantom.

In the first part of this study a computational fluid dynamics model was investigated to simulate the mixing procedure. Mixing techniques of shaking and spinning were simulated using the computational fluid dynamics tool FLUENT. In the second part of this study a Siemens E.Cam gamma camera was simulated using the Monte Carlo software SIMIND. A series of validation experiments demonstrated the reliability of the Monte Carlo simulation. In the third part of this study the simulated the mixing data from FLUENT was used as the source distribution in SIMIND to simulate a tomographic acquisition of the phantom. The planar data from the simulation was reconstructed using filtered back projection to produce a tomographic data set for the activity distribution in the phantom. This completed the simulation routine for phantom mixing and verified the Proof-in-Concept that the phantom mixing problem

can be studied using a combination of computational fluid dynamics and nuclear medicine radiation transport simulations.

Chapter 1 Introduction

1.1 General introduction

Nowadays, medical imaging represents an increasingly important component of modern medical practice [1], which can visualize the inner condition of a patient's body and provides both anatomical and functional information through various modalities. The benefits of medical imaging, such as efficient detection and accurate information, will help the early diagnosis of disease, from which patients can take advantage of available treatments, make proper decisions and decrease both mortality and morbidity of the diseases; hence early diagnosis substantially influence patient treatment strategies, effectiveness of resource utilization and treatment outcome [1].

Nuclear medicine is an important part of medical imaging which provides the basic biochemical information of organ or tissue at the molecular level by tracking the spatial distribution of radiopharmaceuticals introduced into the body [2]; It is very sensitive to pathological changes and capable of detecting early stage disease from abnormal distribution or unusual accumulation of activity. In general, nuclear medicine can be classified into: (1) Single photon imaging. Gamma camera and SPECT (single-photon emission computed tomography) detect the photons emitted from radiopharmaceuticals. In addition, SPECT acquires multiple 2D images from different angles and applies tomographic reconstruction algorithm to create 3D dataset. (2) Coincidence imaging.

PET (Positron emission tomography) which tracks the 511keV photon pair travelling in opposite directions from annihilation. SPECT is the workhorse of the nuclear medicine department [3]. Depending on the clinical situation, the SPECT gamma camera has a wide range of applications through different acquisition modes: planar imaging for bone fracture detection; tomographic acquisition for tumour metastasis analysis; dynamic imaging for kidney function and lung ventilation evaluation; and gated study for cardiac perfusion [4].

Furthermore, radiopharmaceuticals administered to acquire functional information can be specific to different organs and although the pharmaceutical component is small and of negligible side effect, there is always a requirement to keep radiation doses to patients and clinical personnel as low as reasonably achievable (ALARA).

1.2 Reasons for this current study

Routine quality control (QC) tests and the calibration of gamma cameras are necessary in order to consistently acquire good quality images without artefacts [5]. The parameters of gamma camera performance are obtained via QC test phantoms. For example, flood phantoms provide information on intrinsic and extrinsic uniformity; the 4-quadrant bar phantom checks the linearity of the camera system; and the Jaszczak phantom, the standard test phantom for SPECT, examines tomographic specifications, including spatial resolution, contrast resolution, volume sensitivity, rotation axis and many other calibration and reconstruction parameters. In addition, special phantoms,

such as the liver/kidney phantom, have been introduced into the QC procedure to evaluate the integrity of SPECT systems. Those commercially produced phantoms are specifically designed and made by costly material to be capable of precise measurement; at the same time, the high prices limits the affordability.

Mixing radiopharmaceuticals for the phantoms is another of the key components in gamma camera QC procedures, since non-uniform distributions of radiopharmaceuticals within the phantoms will cause distortions and artefacts on the reconstructed images. Currently, there are two major approaches to ensure suitable particle uniformity while preparing phantoms:

- **External mixing**

  The test phantom is filled with pre-mixed solution of radiopharmaceuticals. This method assures the suitable particle distribution, but has the risk of radioactive contamination. In fact, the mixing process within an unsealed container is more dangerous and the radiation safety concerns are more serious than the internal mixing. Although SIEMENS market the MEDISOFT Mixer Trolley System [6], a well shielded system of container, mixer and pump, that is capable of mixing, filling and emptying test phantoms with a high degree of safety; this system is beyond the financial capabilities of many hospitals and research labs.

- **Internal mixing**

  After injecting radiopharmaceutical solution into test phantom, the mixing of radiopharmaceutical and water is performed by shaking (or rolling for Jaszczak phantom) the phantoms manually or by specific tools. Manual mixing cannot ensure the uniformity after mixing because it is not possible to see the radiopharmaceutical. The process is time consuming and most importantly, it will cause unnecessary radiation exposure to the clinical staff, which is against the radiation safety principle of ALARA (As Low As Reasonably Achievable).

1.3 The aims and hypotheses of the current study

Comprehensive quality control of a modern SPECT gamma camera may involve the performance of a large number of sophisticated tests of system function, many of which require costly specialized equipment. [7] The aim of this research was to optimise the quality control procedure to reduce unnecessary radiation exposure of clinical staff. The procedure could be optimized through investigating and improving phantom mixing techniques. Since no additional cost will be introduced, the improvement in mixing procedure could balance the contradiction between the clinical performance and the financial limitation, and most importantly, reduce the health and safety concerns of clinical staff.

Thus, this project was divided in three parts:

- The first part of this study was focused on the radiopharmaceutical mixing methods which included the study of diffusion process in phantoms and the simulation of different mixing techniques through computational fluid dynamic software – FLUENT.

- The second part of this study was targeted on the computational construction and validation of the gamma camera model by using Monte Carlo simulation software – SIMIND.

- The final part of this study linked the computational fluid dynamic simulation and Monte Carlo simulation together to examine the mixing techniques. More specifically, the simulated data of the mixing procedure from FLUENT was validated by the gamma camera model created by SIMIND.

Chapter 2 Background

2.1 Gamma camera

The gamma camera, which was developed by Hal Anger in the 1950's, is the major imaging modality in the nuclear medicine department. The imaging performance of the gamma camera was significantly improved with the development of digital electronics and multiple detector systems; however, the basic components remain unchanged.

Generally, a gamma camera consists of five main components:

1. Collimator, which focuses the gamma sources onto a large transparent NaI crystal.
2. Scintillation crystal (NaI), which converts incoming gamma rays into light.
3. Photomultiplier (PM) tubes and preamplifiers, which convert the light produced by the interaction of the gamma ray and the crystal into an electronic signal.
4. Electronics, such as amplifiers and summation circuits, which combine individual signals and allow calibration of the gamma camera output.
5. Data processing, storage and display unit.

The sketch of a typical gamma camera structure is shown in Figure1.

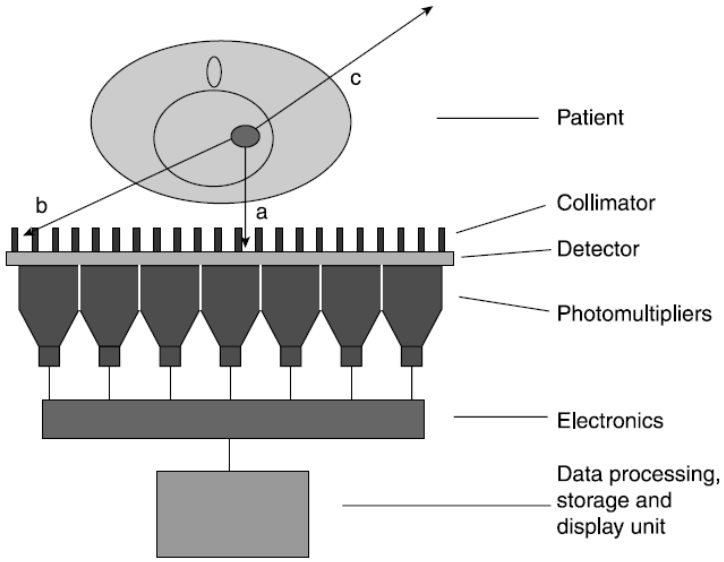

Figure 1 The sketch of a typical gamma camera design.

The collimator of a gamma camera is made of a material with high atomic numbers, such as lead, and is covered with holes which are separated by thin septa. This design ensures that only gamma or x-ray photons traveling approximately perpendicular to the detector are allowed to hit the scintillation crystal. The spatial resolution of the gamma camera is greatly affected by the diameter, length and separation of the holes. Sodium iodide crystal doped with thallium NaI(Tl) is the material used to detect gamma rays. The sodium iodide crystal is a scintillating material that emits light photons when hit by gamma radiations. The intensity of the light photon is proportion to the energy of the radiation. Also, the sodium iodide crystal has almost 100% optical transmission efficiency, which means the intensity loses due to attenuation is very small. Photomultiplier (PM) tubes and preamplifiers convert the light produced by the interaction of the gamma ray and the crystal into an electronic signal.

2.1.1 SIEMENS E.CAM

SIEMENS E.CAM Dual-Detector Variable-Angle Gamma Camera

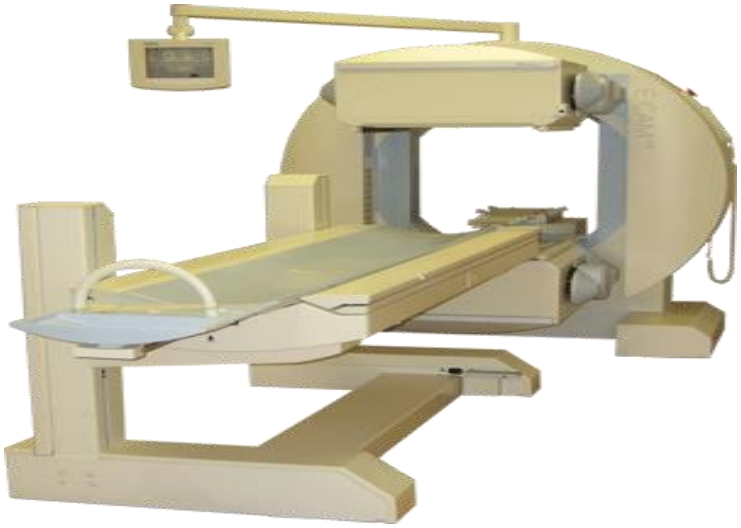

Figure 2 SIEMENS E.CAM Dual-Detector Variable-Angle

The SIEMENS E.CAM Dual-Detector Variable-Angle gamma camera (shown in Figure 2), which is characterized by its high quality in imaging, flexibility and reliability in clinical applications was chosen for this study.

The dual-detectors can be configured into 76 °, 90 ° and 180 ° to optimize the image quality in differently acquisition types, such as whole body, cardiac and general SPECT study.

Several key parameters of the Siemens E.Cam are listed below : [8]

Siemens High-Definition Dynamic Digital Detector

Field-of-View (FOV)	53.3 x 38.7 cm (21 x 15.25 in.)
Diagonal FOV	63.5 cm (25 in.)

Table 1 The field of view and diagonal field of view of Siemens digital detector.

Crystal

Size	59.1 x 44.5 cm (23 x 17.4 in.)
Diagonal	69.2 cm (27 in.)
Thickness	9.5 mm (3/8 in.)

Table 2 The crystal size of the Siemens digital detector.

Siemens Low-Energy High-Resolution (LEHR) collimator

Isotope	99mTc
Hole Shape	Hex
Number of Holes (x 1,000)	148
Hole Length (mm)	24.05
Septal Thickness (mm)	0.16
Hole Diameter (mm across the flats)	1.11
Sensitivity @ 10 cm (cpm/μCi)	202
Geometric Resolution @ 10 cm (mm)	6.4
System Resolution @ 10 cm (mm)	7.4
Septal Penetration (%)	1.5
Focal Length @ Exit Surface (mm)	n.a.
Weight in lb.	45
Weight in kg	20.4

Table 3 The specification of Siemens LEHR collimator.

2.2 Simulation tools

2.2.1 Monte Carlo Simulation

Every step of nuclear medicine imaging involves the phenomena of randomness, from the initial radioactive decay and emission of energy, the interactions with various materials, to the detection of the photons. Monte Carlo (MC) simulations are nowadays employed as an essential tool in nuclear medicine imaging research [9]. MC simulation is a stochastic technique that provides approximate solutions to a variety of mathematical problems by using random numbers and performing statistical sampling experiments [10]. This method has extensive applications in designing new imaging system, improving the accuracy of image reconstruction algorithm, and optimizing practical protocols of SPECT gamma camera. However, in order to acquire a realistic data set, the number of events required in Monte Carlo method is normally large and the calculation process is time consuming, which limits the spread of its application.

A number of Monte Carlo codes for SPECT simulation have been developed to simulate SPECT gamma cameras. Since 1995, seven of them (EGS4, MCNP, SimSET, SIMIND, GEANT, Penelope and GATE), which all have well-validated physics models, geometry modelling tools and visualization utilities, were publicly released (or available from authors)[11]. However, there is no standard code for SPECT and PET that most scientists would agree to use; only SIMIND and SimSET have been predominantly used in the last decade.

2.2.2 SIMIND

SIMIND is specifically developed to SPECT simulation with low energy photons, which could be run on PC and can be downloaded from http://www.radfys.lu.se/simind/. The system is based on Fortran 90, which is a general purpose programming language especially suited to numeric computation and scientific computing. SIMIND code consists of two main programs CHANGE and SIMIND, where CHANGE defines the parameters of the system by graphic user interface and export simulated data; SIMIND reads input parameters and performs the actual Monte Carlo simulation. [12] In addition, the main code could be linked with scoring routines then become capable of parallel computation using MPE command language, which increases the calculation speed significantly [9]. Overall, SIMIND code is easy to access, economical to run, convenient to use and most importantly capable of complex modelling and providing accurate results, therefore, SIMIND was chosen for this project.

2.2.3 FLUENT

ANSYS FLUENT is a general-purpose Computational Fluid Dynamics (CFD) software based on the finite volume method on a collocated grid. The capabilities of dynamic mesh, complex physical model, multiphase process, chemical reaction and post-processing make FLUENT be a powerful tool in industrial design and optimization; hence, it was chosen to simulate and analyse the diffusion and mixing process in the SPECT phantom.

Comprehensive FLUENT simulations have high requirements on computer power. The simulated volume was divided into smaller cells and the changes in diffusion parameter within all cells were tracked by continuous calculations with time; the smaller the cell and time step, the more accurate the simulation. For example, the mixing simulation of a phantom divided into 520,000 cells and 0.01 second time step for 30 minutes period will take more than one week to complete in a normal computer with a 2G Hz processor.

2.2.4 Other tools

ImageJ

ImageJ is a public domain, Java-based image processing program developed at the National Institutes of Health. ImageJ has several advanced features compared to other image analysis tools:

- File Formats:

ImageJ could support most of major file formats of image: such as DICOM (Digital Imaging and Communications in Medicine), GIF, JPEG, BMP, PNG, PGM, FITS and ASCII.

- Data Type:

ImageJ could process the images in 8-bit grayscale or indexed colour, 16-bit unsigned integer, 32-bit floating-point and RGB colour.

- Computing speed:

ImageJ is world's fastest pure Java image processing program, which could process 40 million pixels per second

- Analysis:

ImageJ could provide most of the useful measurements in the analysis, such as area, mean, standard deviation, min and max of a selection or entire image etc.

The ImageJ used in this research was:

ImageJ 1.47 bundled with 64-bit Java (25MB; requires 64-bit Windows). [13]

All versions of ImageJ are available at http://rsbweb.nih.gov/ij/download.html.

MATLAB

MATLAB® is a high-level language and interactive environment for numerical computation, visualization, and programming. MATLAB® was developed by MathWorks. It allows matrix manipulations, plotting of functions and data, implementation of algorithms, creation of user interfaces, and interfacing with programs written in other languages, including C, C++, Java, and FORTRAN.

The MATLAB package used in this study was MATLAB 7.12.0 (R2011a).

2.3 Physical Phantoms

2.3.1 NEMA line source phantom

NEMA, the National Electrical Manufacturer's Association, has established definitions, quantitative measurements of performance characteristics, and reporting techniques for the specification of scintillation camera based single photon emission computed tomography (SPECT). The line source phantom is made for the spatial resolution measurements of NEMA specifications. [14]

The phantom consists of an acrylic cylindrical chamber and three line sources. The inside diameter of the chamber is 20 cm; the thickness of wall is 0.635 cm and the inside length is 20 cm. The inner diameter of the line source is 1mm and the length is 20 cm. In this study, only the line source phantom was used in the spatial resolution experiment.

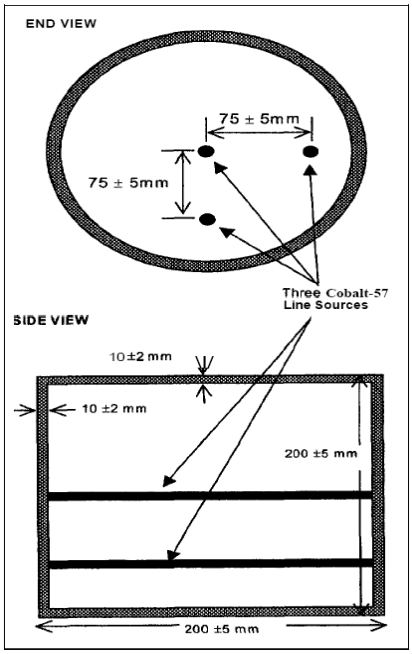

Figure 3 The NEMA line source phantom used in the spatial resolution experiment.

2.3.2 IEC count rate performance in scatter phantom (insert phantom)

IEC count rate performance in scatter phantom is shown in Figure 4. It is used for a number of validation measurements for NEMA performance testing. The phantom contains a disk phantom (insert phantom) and a larger Perspex phantom. The disk phantom is designed to be filled with a radioactive source to be imaged alone, or placed inside the Perspex phantom. The outer diameter of the insert phantom is 15 cm, the height is 1.1 cm; the inner diameter of the insert phantom is 13 cm, the height is 1 cm [15].

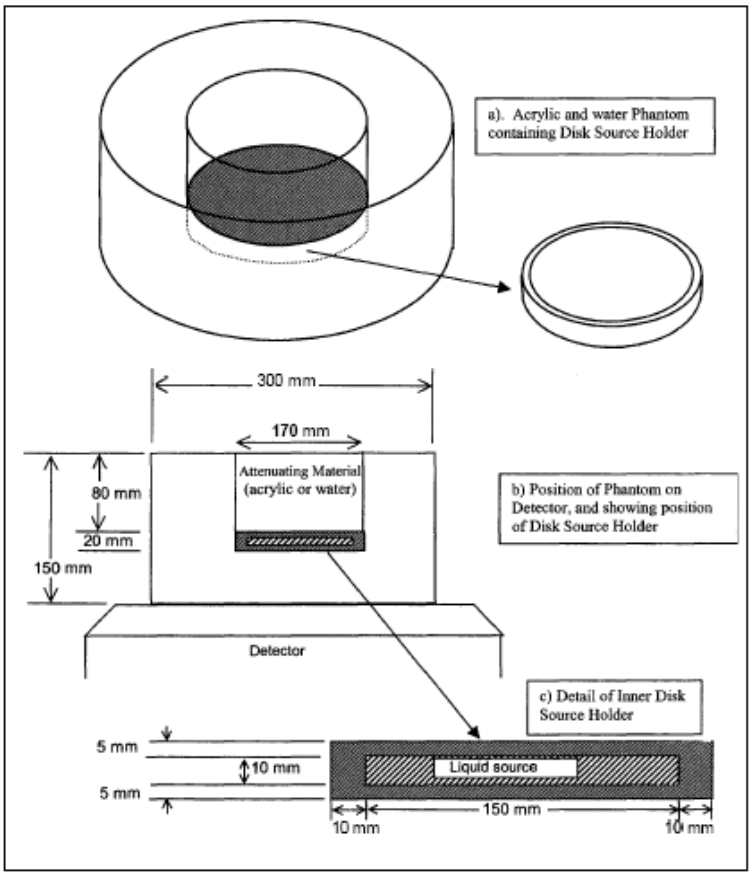

Figure 4 The IEC Count Rate Phantom (insert phantom) used in experiment.

2.3.3 Nuclear Associates PET/ SPECT Phantom Source Tank, Phantom Insert and Cardiac Insert

The Nuclear Associates PET/SPECT Phantom allows tomographic measurements for performance testing. It permits measurements of the resolution of "hot" lesions in a cold field, "cold" lesions in a "hot" (or radioactive) field, linearity, uniformity of response to a uniform field, and a simple way to check the center of rotation. [16]

In this study, only source tank was used in the experiments. The source tank is made of acrylic and has an o-ring sealed cover with fill and drain ports. The outer diameter of the source tank is 21.95 cm; the inner diameter of the tank is 20.32 cm and the height of the phantom is 31.75cm.

Figure 5 Nuclear Associates PET/ SPECT volume phantom.

Chapter 3 Fluid Dynamics and FLUENT simulation

3.1 Introduction

Mixing fluid is a complicated fluid dynamic problem, which could be based on a number of mechanisms, such as agitation, sparging to static flow manipulation [17]. The goal of mixing is to break the strands of fluid to a sufficiently small size to make the mixture homogenized [18].

3.2 Conservation equations and mixing model

3.2.1 Conservation equations

The mixing process could be initiated by many factors, such as the external force that create turbulence, the heat that increases the volume of gas and the chemical reaction that changes the viscosity of a fluid. In fluid dynamics the mixing processes are described by a set of conservation equations, where these equations track the changes in the fluid that result from convection and diffusion. For complicated cases, these equations can be coupled together to indicate that change in one variable may lead to changes in other variables. The conservation equations are the theoretical basis of all simulation in computational fluid dynamics (CFD).

For example, the continuity equation is used to describe the conservation of mass; the momentum equation is used to describe the conservation of momentum. However, the set of conservation equations used to describe the fluid dynamic case is too complicated to derive and calculate by hand; fortunately, modern computer technology and CFD software, such as FLUENT, are introduced to analyse, solve and even simulate the problems.

3.2.2 Auxiliary models

Although a wide range of applications can be described by the set of conservation equations, problems that involve more complex situations require the assistance of additional models. In this study, a multiphase model was used to simulate the mixing process of radiopharmaceuticals in a volume phantom.

Multiphase Models

A large number of flows encountered in nature and technology are a mixture of phases, where gas, liquid, and solid are three basic physical phases of matter. In multiphase flow, phase is classified not only by identifiable characteristics but also the particular inertial response and interaction with the flow of materials. For instance, same solid particles in different sizes can be treated as different phases, since the dynamic responses to the flow are different for each. In order to simulate multiphase problems, the process should begin with the classification of flow regimes and determination of simulation models which involve different degrees of interphase coupling. There are

four categories of flow in multiphase regime: gas-liquid or liquid-liquid flows; gas-solid flows; liquid-solid flows; and three-phase flows. In this study, gas-liquid or liquid-liquid flows and three-phase flows were investigated in detail, where three-phase flows are the combination of the other flow regimes (i.e. are more complex)[17].

There are currently two approaches for the numerical calculation of multiphase flows: the Euler-Lagrange approach and the Euler-Euler approach. The Euler-Lagrange approach is normally used for the discrete phase modeling, which is not suitable for the simulation of mixing. The Euler – Euler approach can be applied to fluid mixing.

The Euler-Euler Approach

In the Euler-Euler approach the different phases are treated mathematically as interpenetrating continua. Since the volume of a phase cannot be occupied by the other phases, the concept of phasic volume fraction is introduced. These volume fractions are assumed to be continuous functions of space and time and their sum is equal to one.

Conservation equations for each phase are derived to obtain a set of equations, which have similar structure for all phases. These equations are closed by providing constitutive relations that are obtained from empirical information.

Three different Euler-Euler multiphase models are available in Fluent:

1. Volume of Fluid (VOF) Model

   This model is designed for two or more immiscible fluids and focus on the interface between fluids, which is not suitable for this study.

2. Mixture Model

   This model is designed for two or more phases of fluids.

3. Eulerian Model

   This model is the most complex multiphase models in FLUENT, which solves a set of momentum and continuity equations for each phase.

Comparing the performance of mixture model and the Eulerian model, the Eulerian model usually provides more accurate results than the mixture model, since more conservation equations are solved. On the other hand, the mixture model requires less computational resources, because it solves fewer conservation equations. The choice of proper simulation model is a trade-off between simulation accuracy and simulation time. The simulation time was a critical issue for this study and the accuracy requirements could be relaxed for this proof-of-concept research. Therefore, the Euler-Euler multiphase mixture model was chosen for the FLUENT simulation in this study.

3.2.3 Mixture model theory and equations

The mixture model is a simplified multiphase model that can be used to model multiphase flows where the phases move at different velocities, but assume local

equilibrium over short spatial length scales [18]. The mixture model allows the phases to be interpenetrating. The volume fractions of different materials for a control volume can therefore be equal to any value between 0 and 1, depending on the space occupied by different phases. The mixture model solves the continuity equation, the momentum equation and the energy equation for the mixture, and the volume fraction equation for the secondary phases.

Continuity equation

The continuity equation for the mixture is [19]:

$$\frac{\partial}{\partial t}(\rho_m) + \nabla \cdot (\rho_m \vec{v}_m) = 0$$

The v_m is the mass-averaged velocity and can be calculated from:

$$\vec{v}_m = \frac{\sum_{k=1}^{n} \alpha_k \rho_k \vec{v}_k}{\rho_m}$$

The ρ_m is the mixture density and can be calculated from:

$$\rho_m = \sum_{k=1}^{n} \alpha_k \rho_k$$

Where α_k is the volume fraction of phase k and ρ_k is the density of this phase.

Momentum equation

The momentum equation for the mixture can be obtained by summing the individual momentum equations for all phases.

The momentum equation for mixture model is shown below [19]:

$$\frac{\partial}{\partial t}(\rho_m \vec{v}_m) + \nabla \cdot (\rho_m \vec{v}_m \vec{v}_m) = -\nabla p + \nabla \cdot \left[\mu_m \left(\nabla \vec{v}_m + \nabla \vec{v}_m^{\mathrm{T}}\right)\right] + \rho_m \vec{g} + \vec{F} + \nabla \cdot \left(\sum_{k=1}^{n} \alpha_k \rho_k \vec{v}_{\mathrm{dr},k} \vec{v}_{\mathrm{dr},k}\right)$$

The n is the number of phases, F is body force.

The μ_m is the viscosity of the mixture and can be calculated from:

$$\mu_m = \sum_{k=1}^{n} \alpha_k \mu_k$$

The $v_{dr,k}$ is the drift velocity for secondary phase k and can be calculated from:

$$\vec{v}_{\mathrm{dr},k} = \vec{v}_k - \vec{v}_m$$

Energy equation

The energy equation of mixture model is shown below [19]:

$$\frac{\partial}{\partial t} \sum_{k=1}^{n} (\alpha_k \rho_k E_k) + \nabla \cdot \sum_{k=1}^{n} (\alpha_k \vec{v}_k (\rho_k E_k + p)) = \nabla \cdot (k_{\mathrm{eff}} \nabla T) + S_E$$

where k_{eff} is the effective conductivity and the first term on the right hand side is the energy transfer due to conduction; S_E is the energy transfer from volumetric heat sources.

Volume fraction equation

From the continuity equation for secondary phase p, the volume fraction equation for secondary phases p can be obtained[19]:

$$\frac{\partial}{\partial t}(\alpha_p \rho_p) + \nabla \cdot (\alpha_p \rho_p \vec{v}_m) = -\nabla \cdot (\alpha_p \rho_p \vec{v}_{\mathrm{dr},p}) + \sum_{q=1}^{n} (\dot{m}_{qp} - \dot{m}_{pq})$$

where m_{qp} and m_{pq} are the relative mass fraction of phase p and q.

3.3 The difficulties and assumptions

3.3.1 Difficulties

There are many difficulties in the simulation of phantom mixing for quality control experiments.

- Lack of reference

Little research has been done to investigate the phantom mixing problem in clinical use. There did not appear to be any research published on the use of CFD tools, such as FLUENT, to simulate the mixing of radiopharmaceuticals in a phantom.

- Lack of data

It was not possible to find several key properties of the radiopharmaceutical sodium pertechnetate typically used for quality control measurement. For example, the viscosity of $NaTcO_4$ solution is unknown, since it is not a popular subject in computational fluid dynamics and there is no reference related to this.

Pertechnetate (TcO_4^-) is a soluble compound of Technetium (Tc) and is used to carry radioactive isotope Technetium 99m (Tc-99m) in nuclear medicine scans and QC procedures. For clinical applications, Technetium 99m is usually produced in a generator containing Molybdenum-99 (Mo-99). Since saline (0.9%NaCl solution) is used to "wash out" TcO_4 from the on-site a generator, the product of the generator is a mixture of saline and $NaTcO_4$. In a typical elution from a generator, 6ml solution with 40GBq activity indicates that there are about $9.28x10^{-4}$ mol NaCl and only $2.08x10^{-9}$

mol $NaTcO_4$, the proportion difference is massive. It was not possible to simulate the mixing of a mixture that already contained two materials with such a huge proportion difference.

3.3.2 Assumptions

Several assumptions were needed to make this simulation possible.

- Assumption 1:

The solution containing $NaTcO_4$ and NaCl from the generator is 'well' mixed, which means the TcO_4- and Cl- distribute uniformly within the volume.

- Assumption 2

The radii of Tc^{7+}, Cl^- and O^{2-} were listed below in Table 4.

Particles	Radius (Angstrom)
Tc^{7+}	0.56
Cl^-	1.81
O^{2-}	1.38

Table 4 The radii of Tc^{7+}, Cl^- and O^{2-} (where 1 Angstrom = 100 Pico meter)

The TcO_4- is a typical tetrahedral molecule with bond angle of 109.5 degrees; hence the radius of TcO_4- is around 1.9 Angstrom, which is very close to the radius of Cl^-. Therefore, it was assumed that TcO_4- and Cl- would mechanically have similar or

even the same characteristics in the mixing procedure. If so, the distribution of NaCl in the mixed phantom could be treated as the distribution of $NaTcO_4$. i.e. The simulation problem of TcO_4- could be simplified to the simulation of 0.9% NaCl solution (Saline), where all of the saline properties were available for a FLUENT simulation.

- Assumption 3

To further simplify the simulation, the temperature of the water in phantom, temperature of the air and temperature of saline were assumed to be exactly the same. i.e. there was no heat transfer at all.

Based on these three reasonable assumptions, the simulations of radiopharmaceutical mixing were performed in FLUENT.

3.4 Fluent settings

3.3.1 Software version and computing resources

Software version

- FLUENT

Two FLUENT packages were studied in this project:

FLUENT 6.3.26 was chosen to match the FLUENT version of the 'Blue Fern' super computer at the University of Canterbury.

FLUENT 14.0 was used to apply several complex user defined functions (UDF) simulations in the final stage of this study.

- GAMBIT

GAMBIT 2.3.16 was introduced as the tool of building 'mesh' for FLUENT simulations.

- TECPLOT

TECPLOT360 2010 was chosen for the data analysis and post processing of the FLUENT results.

Computational resources

- The FLUENT simulation was performed by a SONY NR series Laptop with Intel Pentium Dual Core Processor (1.86 GHz); the operating system was Windows® Vista Home Premium.

- Blue Fern, which is a collegial, high performance e-research computing service facility based at the University of Canterbury, was used to reduce the simulation time [20]. However, this computational resource was later abandoned since the version change of FLUENT installed in Blue Fern was incompatible with the UDF methods developed for complex mixing.

3.3.2 Settings

Materials

The multiphase mixture model was used for this FLUENT simulation. The three phases were air in the phantom, water in the phantom and saline injected into the phantom. Hence, the basic parameters for the three materials must be defined in FLUENT and were set to the values shown in Table 5.

	Density(kg/ m^3)	Viscosity (kg/m -s)
air	1.225	$1.789e^{-5}$
water	998.2	0.001003
saline	1006.2	0.00103

Table 5 The density and viscosity of air, water and saline.

The viscosity of water and saline are very similar and they have been treated as identical in some research [18].

Operating Conditions

As shown in Figure 6, the operating pressure was set to one standard atmosphere pressure (101325 Pascal) and the gravitational acceleration was set to 9.81m/s^2 in a direction along the negative z axis.

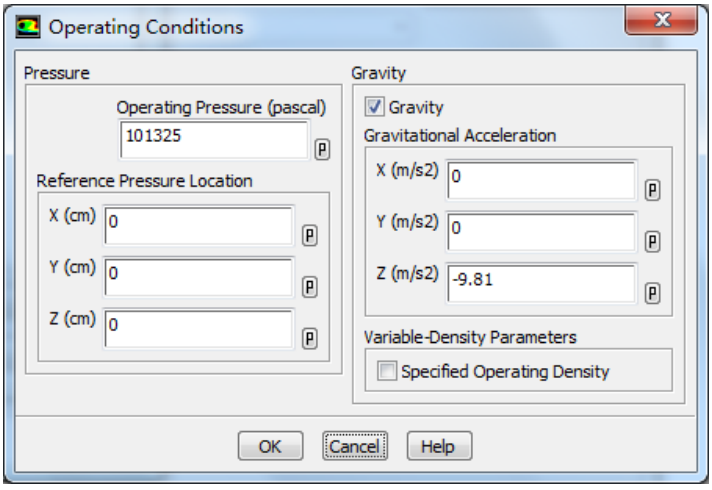

Figure 6 The settings for the FLUENT operation conditions.

Model

As shown in Figure 7, the mixture model was chosen under the multiphase model and the number of Eulerian phases was set to 3 to perform the three phase simulation.

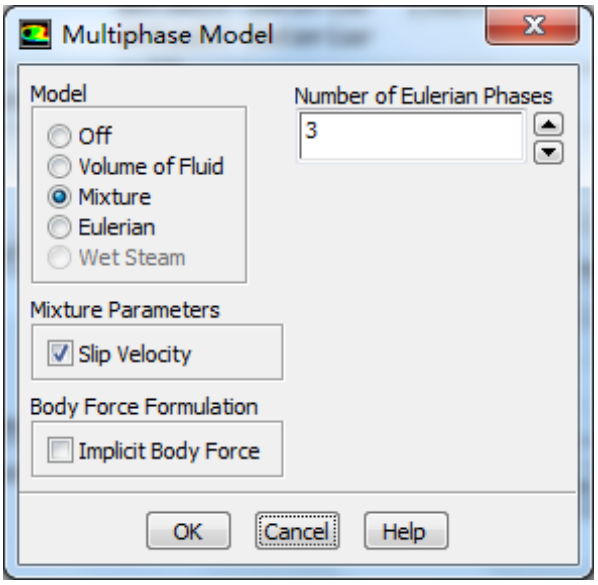

Figure 7 The settings for the Multiphase Model.

Viscous

In the viscous model setting for turbulent flow, the standard k-epsilon model was chosen. The standard k-epsilon model is the most widely used model and has been studied for many years. It is both robust and economical in computational resources. Most importantly, rapid simulation is one of the main advantages of this model, which filled the need of reducing simulation time, especially after the computational source of Blue Fern was abandoned.

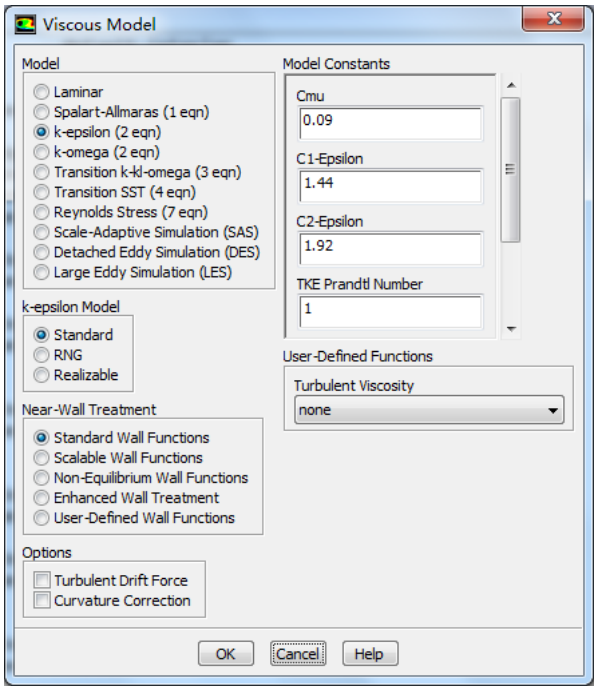

Figure 8 The settings for Viscous Model.

Phases

The three phases in the simulation were defined in this section:

Air was defined as primary phase (phase 1);

Water was defined as secondary phase (phase 2);

Saline was defined as secondary phase (phase 3).

Boundary Condition

Figure 9 shows the boundary condition setting for the simulation.

The stationary wall was chosen and ‘no slip’ was set to the shear condition, since in viscous flows the no-slip boundary condition is enforced at walls by default [19].

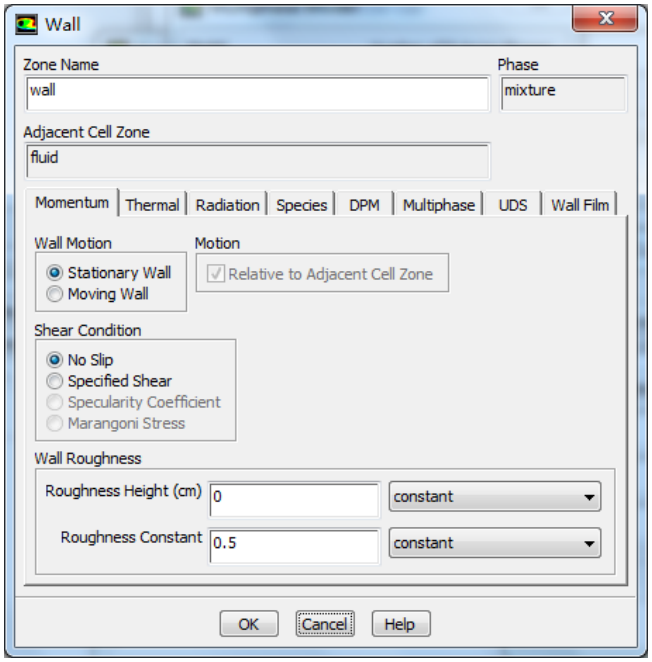

Figure 9 The settings for boundary conditions.

3.5 Grids for phantoms

FLUENT is an unstructured solver that uses internal data structures to assign an order to the cells, faces, and grid points in a mesh and to maintain contact between adjacent cells [19]. This provides the flexibility to use the best grid topology for the problem. FLUENT can import different types of grids from various sources and GAMBIT is one of most popular tools to manipulate the grid. The four views of the mesh for the two phantoms in this study were illustrated by GAMBIT in Figure 10 and Figure 11. The mesh size and information was examined using the FLUENT commands 'Mesh Info' and 'Mesh Size', and mesh quality was checked using 'Mesh Check'.

3.51 Mesh of the IEC insert phantom

Mesh check

x-coordinate: min(m) = - 7.50000e -02, max(m) = 7.50000e -02

y-coordinate: min(m) = - 7.50000e -02, max(m) = 7.50000e -02

z-coordinate: min(m) = 0.0000e, max(m) = 1.1650000e -02

Mesh size

Level	Cells	Faces	Nodes	Partitions
0	6774	22687	9232	1

Mesh quality

The minimal orthoganol quality = 5.67298e-01, where orthoganol quality ranges from 0 to 1 and values close to 0 correspond to low quality.

The mesh quality was considered poor and this small phantom was only used as a test phantom to observe the mixing trends.

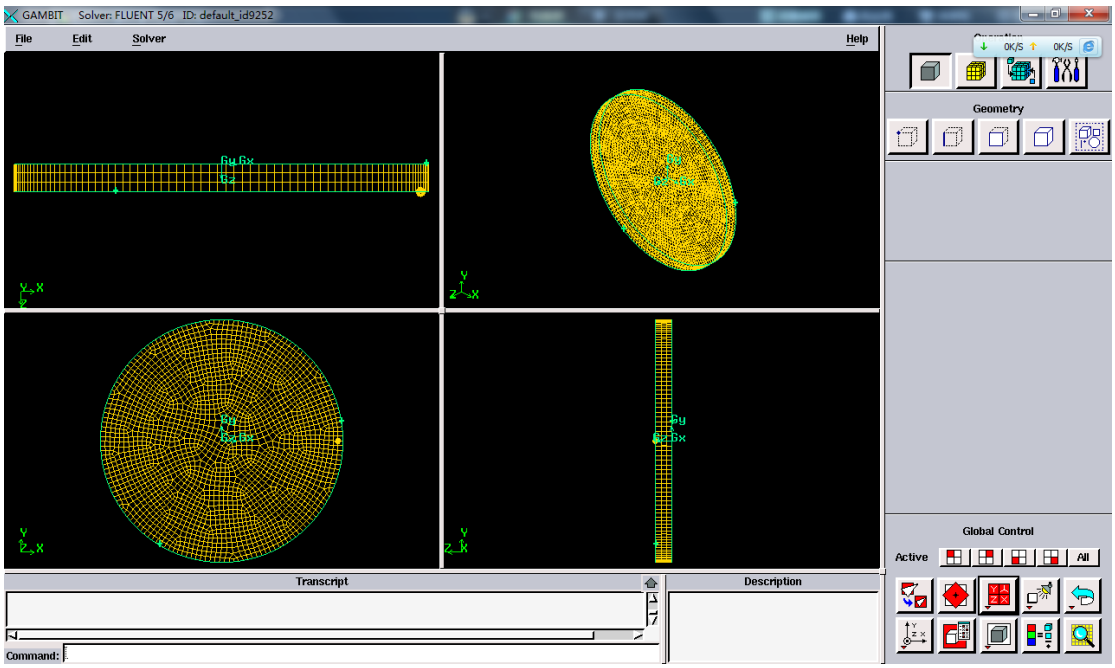

Figure 10 The mesh for the IEC insert phantom.

3.5.2 Mesh of IEC Nuclear Associates SPECT volume phantom (model 76-823)

Mesh check

x-coordinate: min(m) = - 1.150000e -01, max(m) = 1.150000e -01

y-coordinate: min(m) = - 1.15000e -01, max(m) = 1.150000e -01

z-coordinate: min(m) = 0.0000e, max(m) = 3.050000e -01

Mesh size

Level	Cells	Faces	Nodes	Partitions
0	**228382**	**695119**	**238524**	**1**

Mesh quality

The minimal orthoganol quality = 8.83360e-01, where orthoganol quality ranges from 0 to 1 and values close to 0 correspond to low quality.

The quality of the mesh (Figure 8) is good for accurate simulations, and this phantom was used as the main phantom in this study.

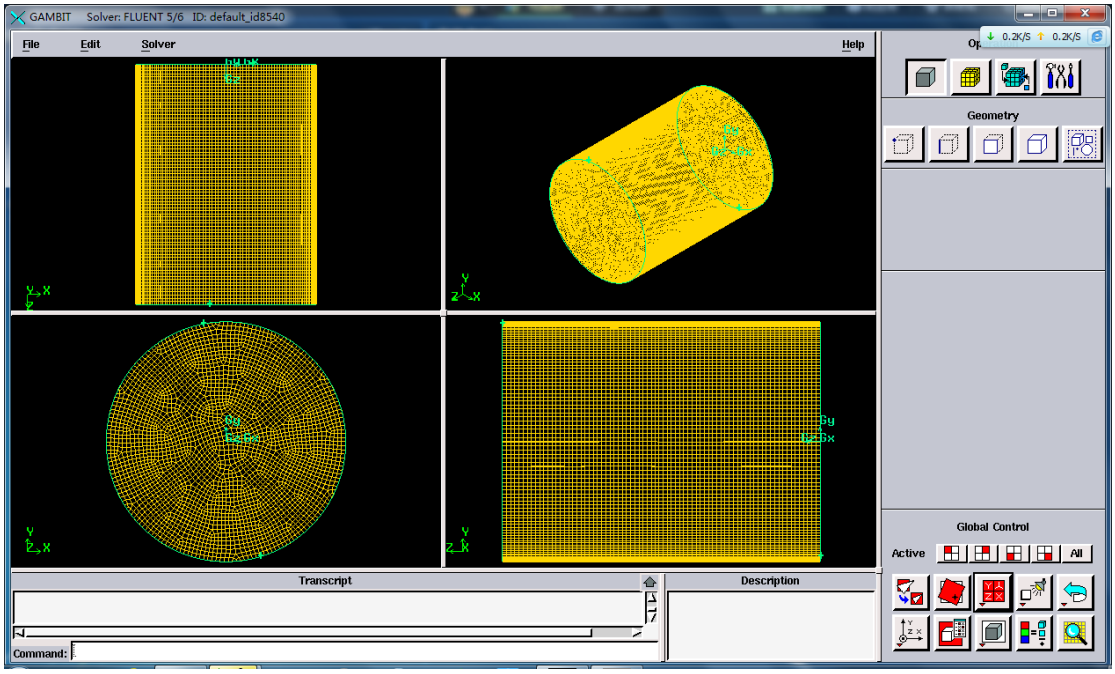

Figure 11 The mesh for the source tank of IEC Nuclear Associates SPECT volume phantom.

3.6 Experiments

Experiments were performed to demonstrate the problems with phantom mixing and relying simply upon diffusion to cause mixing. The main phantom of interest is a volume phantom for SPECT measurement. It would be preferable to perform dynamic tomographic imaging to demonstrate diffusion or mixing over a long sampling interval, but this facility was not available. Instead, planar dynamic imaging was performed using the gamma camera heads at a 90 degree configuration.

3.6.1 Diffusion experiment

Camera and phantom setup

The radiopharmaceutical diffusion experiment was performed using a Siemens E.Cam gamma camera, where Detector1 was set to 0 degree and Detector2 was set to -90 degree.

The SPECT volume phantom was used in this static acquisition. The source tank phantom was filled with water and was left still on the table for 20 minutes to reduce the turbulence within the phantom as much as possible. The detailed setup is shown in Figure 12.

Figure 12 the camera and phantom setup for the diffusion experiment.

Source

Tc99m from the generator at Christchurch Hospital was used as the radioactive source. The total Tc99m activity was 315MBq; and the residual activity was 85.6 MBq, hence, 229.4 MBq was injected in to the source phantom through a BD 1ml Syringe with 23 gauge needle [21].

Acquisition

Dynamic images of 128 x 128 were taken using the E.Cam and with two phases of:

- 1 frame per second for 30 frames;
- 1 frame per minute for 30 frames.

Hence the acquisition time was 30min and 30second and a total of 60 images.

Result

The DICOM file from E.Cam was imported into ImageJ for analysis. Because of the low activity in the phantom and the relatively short acquisition times per frame, the counts on both detectors were low. Windowing and levelling were used to enhance the image in ImageJ. The processed images are illustrated in Figure 13.

The image on the top left was the 5^{th} image. In order to minimize the turbulence, the injection process was slow and gentle. The syringe can still be observed in this image.

The image on the top right was the 30^{th} image. The diffusion process was slow, the outline of injected radiopharmaceutical could still be observed after 30 seconds.

The image on bottom left was the 31^{th} image. One minute from the previous image, the injected radiopharmaceutical had 'sunk' to the bottom of the phantom.

The image on the bottom right was the 60^{th} image. The diffusion trend of the injected radiopharmaceutical could be observed clearly. The trend of sinking continued and the radiopharmaceutical began to spread along the bottom surface after hitting the bottom of the source phantom.

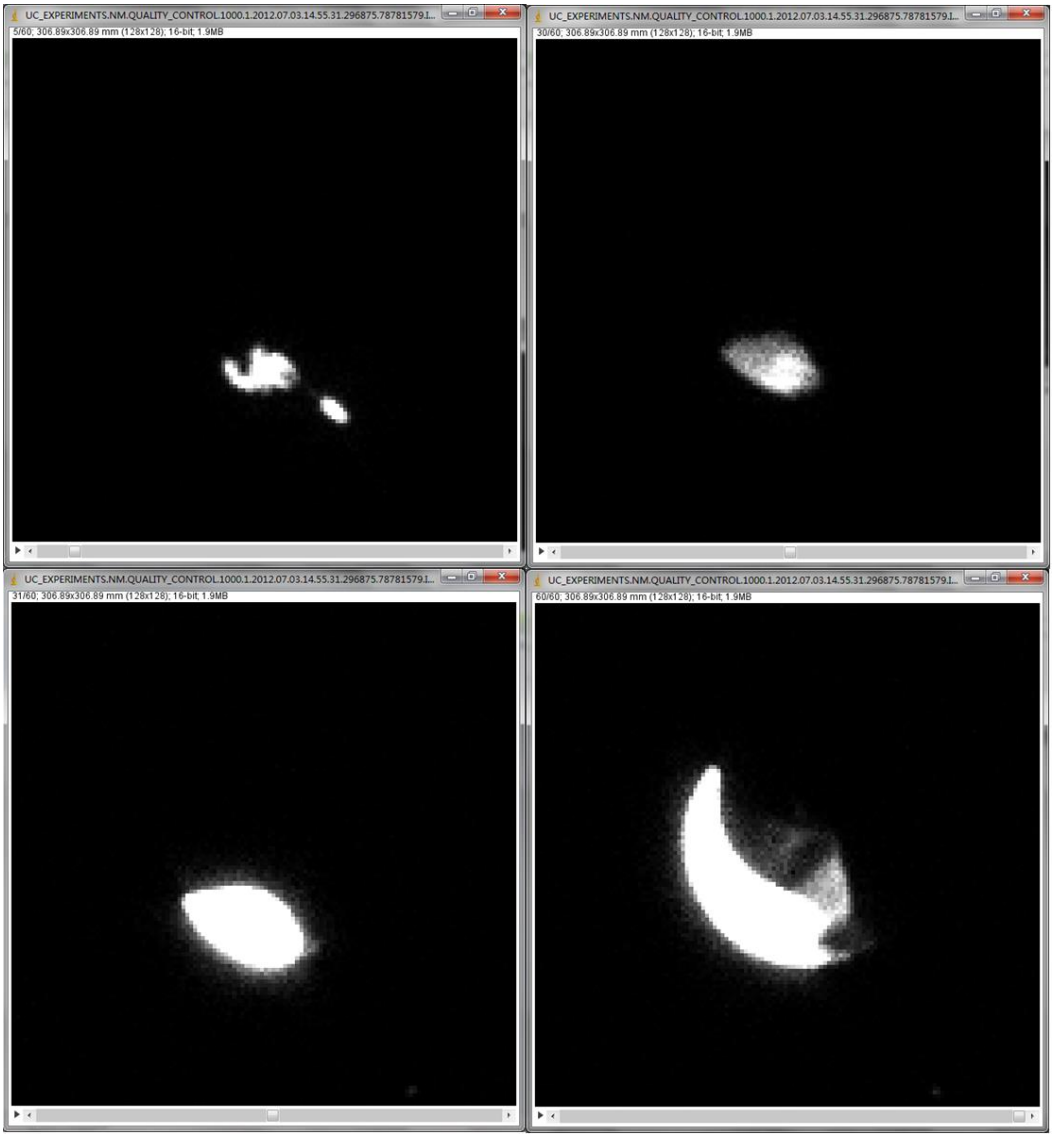

Figure 13 The images taken by detector1 at 5s, 30s, 1m30s and 30m 30 s of experiment. (This is a top view of the phantom).

The activity sinks to the bottom of the phantom (as seen from lateral images) then continues to spread along the bottom of the phantom.

3.6.2 Phantom rotation experiment

Camera and phantom setup

The phantom rotation experiment was performed using the Siemens E.Cam gamma camera with the Detector1 was set to 0 degree and the Detector2 was set to -90 degrees.

The SPECT volume phantom was used in this acquisition. The phantom was filled with water and left at room temperature for a day. The phantom was placed on a dynamic phantom rotor and rotated for 15 minutes to create flow within the phantom. The rotation rate of the rotor was 1.02 rotations/s. Figure14 shows the setup details.

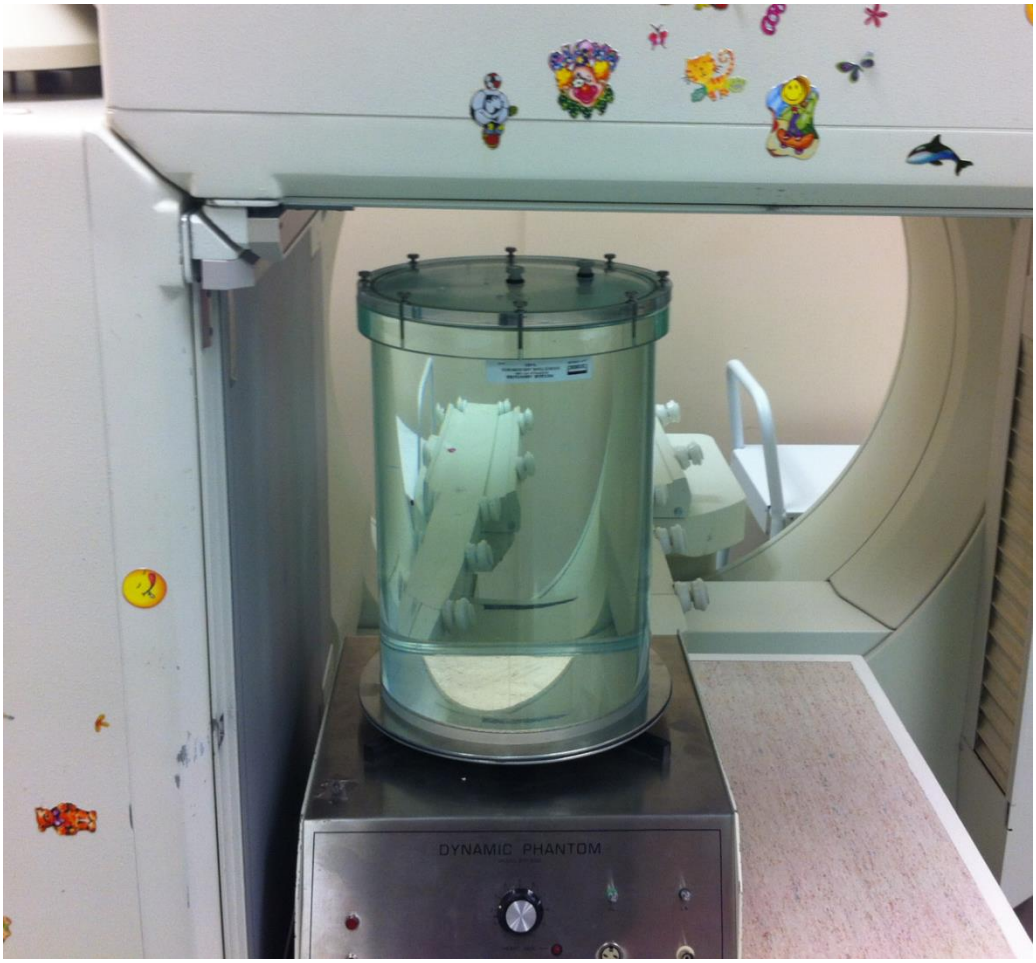

Figure 14 The camera and phantom setup for the phantom rotation experiment.

Source

Tc99m was the radioactive source in this experiment. The total activity of the Tc99m used was 354MBq; and the residual activity was 70.8MBq, hence, 283.2 MBq was injected in to source phantom through a winged infusion set 23G x 3/4" taped to the top of the phantom so the activity could be injected as soon as the rotation of the phantom was stopped at 15 minutes.

Acquisition

Dynamic images of 128 x 128 were taken using Siemens E.Cam gamma camera:

- 1 frame per 5 seconds for 30 frames;
- 1 frame per minute for 30 frames.

Hence the acquisition time was 32min and 30second and a total of 60 images for each detector.

Result

The DICOM file from E.Cam was imported into ImageJ for analysis. Because of the low activity in the phantom and the relatively short acquisition times per frame, the counts on both detectors were low. Windowing and levelling were used to enhance the image in ImageJ. The processed images are illustrated in Figure 15 for Detctor1 and Figure 16 for Detector2. From Figure 15 and Figure 16, the trends of water flow and radiopharmaceutical mixing was confirmed through the experiment. These planar images show reasonable mixing after 32 minutes and 30 seconds when the volume phantom was rotated before injecting the radiopharmaceutical into the phantom.

The source tank was accelerated by the rotor and the water inside was rotated with the phantom, hence the water near the wall moved faster than water near the centre of the source tank. From the Detetcor1 images, the outer part of the volume tank had the distribution of radiopharmaceutical right after the injection and the central part of the tank contained very little activity for a long time. When the rotor was stopped and the image acquisition was started, the water inside the source tank didn’t stop instantly, as observed by small amounts of dust suspended in the water. The water just slowed by the friction of the wall and the centripetal force pushed the water to the top of the tank; in fact, the tank was not fully filled, there was a 2 cm gap from water surface to the top of the phantom. Therefore, a circular flow of water from top to the bottom in the phantom was created, which could transfer the radiopharmaceutical from top to the bottom much quicker. However, the circular flow along the phantom wall was still the dominant flow in the phantom.

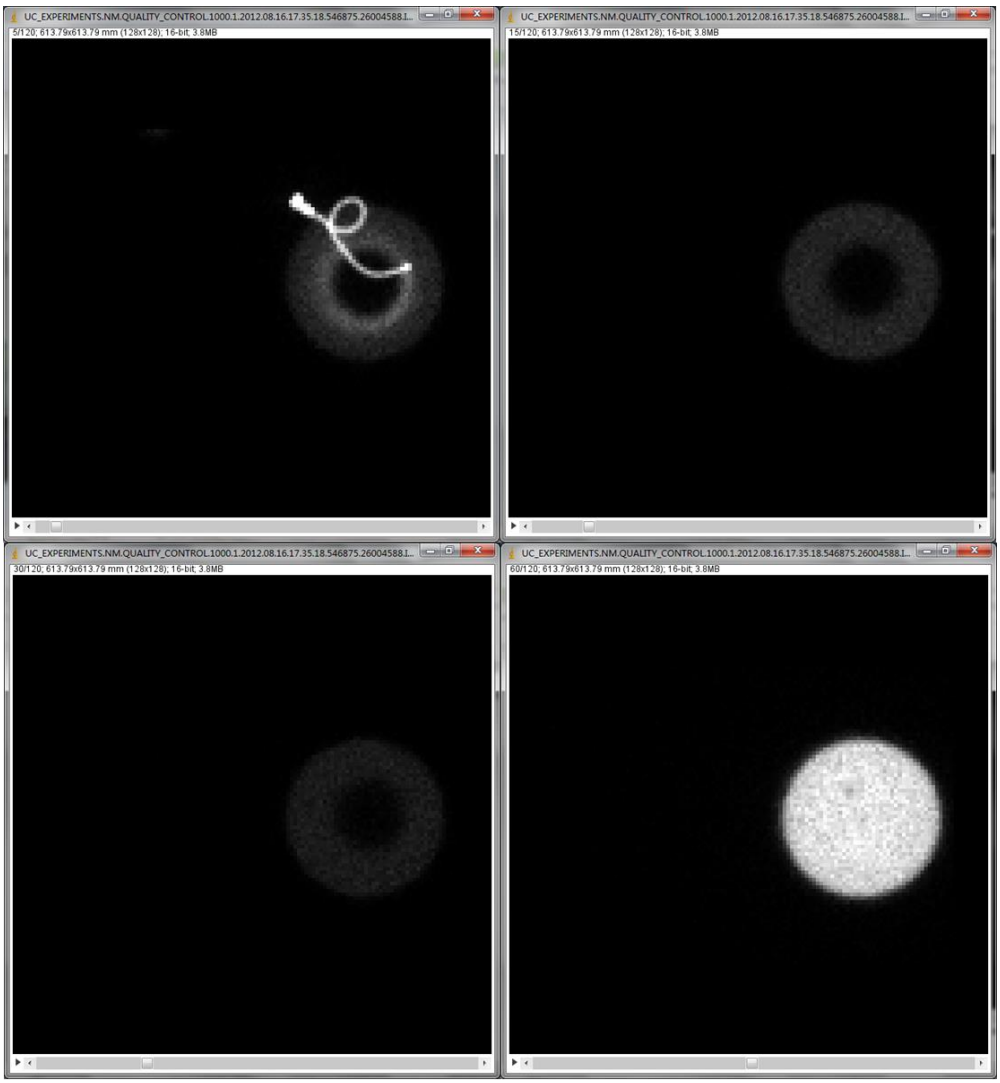

Figure 15 The images taken by Detector1 at 25s, 75s, 2m30s and 32m30s of the experiment.

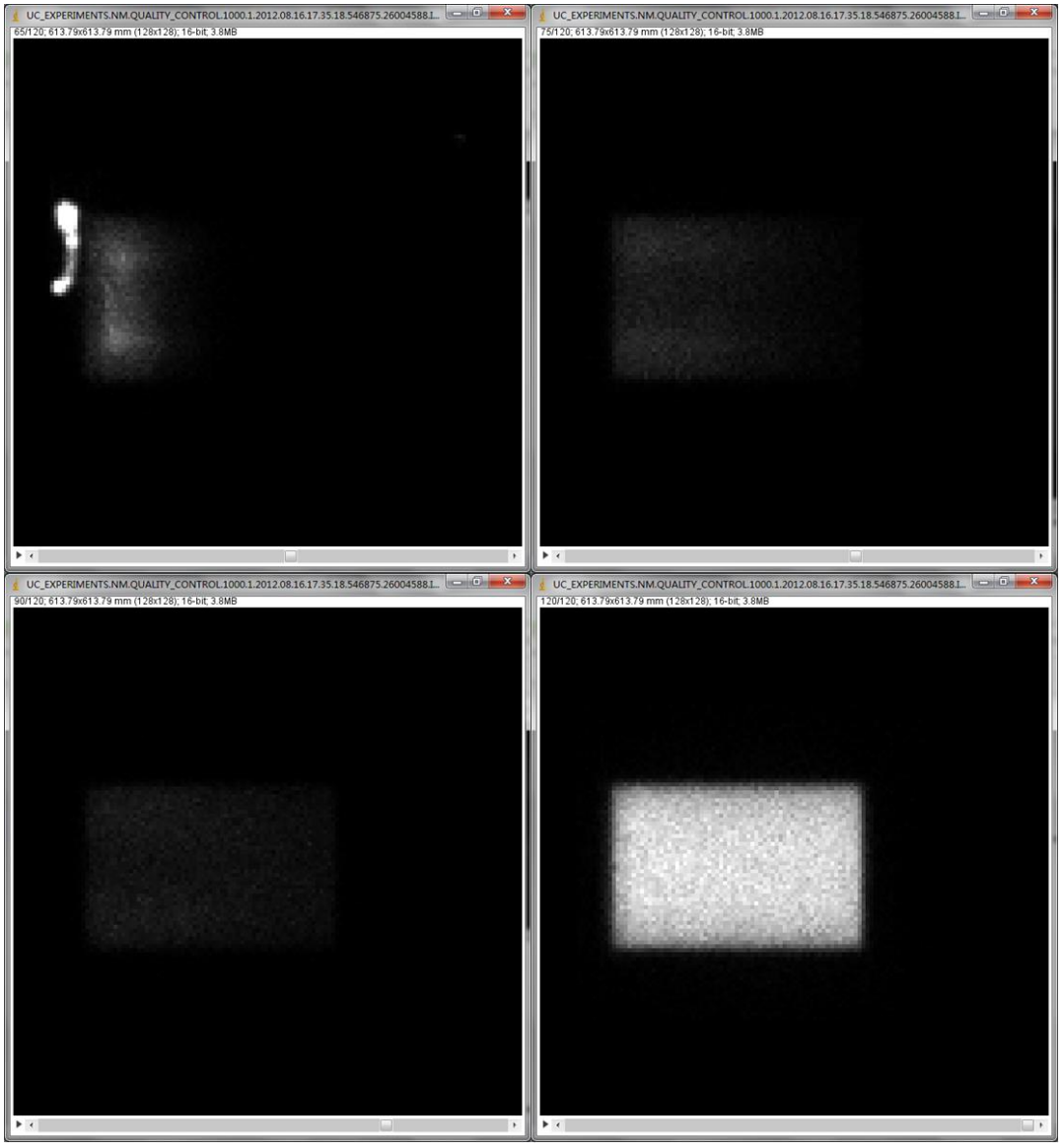

Figure 16 The images taken by Detector2 at 25s, 75s, 2m30s and 32m30s of the experiment. (The left hand side is the top of the phantom.)

3.7 FLUENT Simulation

3.7.1 Residual

In the CFD simulation, the solution of the conservation equation set may be considered converged when there is no perceptible change in the dependent variables from one iteration to another, with the residual used to measure the difference in the solutions for two successive iterations. In fact, the residual will become smaller and smaller, since the input for one iteration is simply the solution to the previous iteration. Eventually, the residual values will become small enough to make the simulation achieve convergence [22].

3.7.2 User Defined Function (UDF)

The user defined function is a function that can be dynamically loaded with customized settings into the FLUENT solver to enhance the standard features of the program. The user defined function for FLUENT simulation can be written in the C language on any text editor. With the help of user defined functions, more complex mixing procedures could be simulated.

Controlled Spinning (rotation)

In the user defined function 'controlledSpinning.c' (shown in appendix 1), the rotation rate and the rotation time of the SPECT volume phantom were defined through a transient profile function: the rotation (or spinning) rate was set to 0.5 rad/s and the

rotation time was set to 60 seconds. The mixing method of spinning the phantom for 60 seconds only at the rate of 0.5 rad/s was also simulated.

Result:

The time step for the rotation simulation was 0.1 second and the iteration number for each step was 20. Some of the simulated results at selected times were loaded to TECPLOT360 for further analysis.

The vector of each node (at 0.1 s) from the mesh of the SPECT volume phantom is plotted in Figure 17. Although the rotation of this simulation was different to the experiment, the general behaviour observed in the experiment was shown by using TECPLOT. The vectors near the edge of the phantom were moving along the wall, and the lengths of vectors were decreasing while moving towards the centre of the phantom. Also, the trend of the circular flow from top to bottom of the phantom could be observed on the vector map.

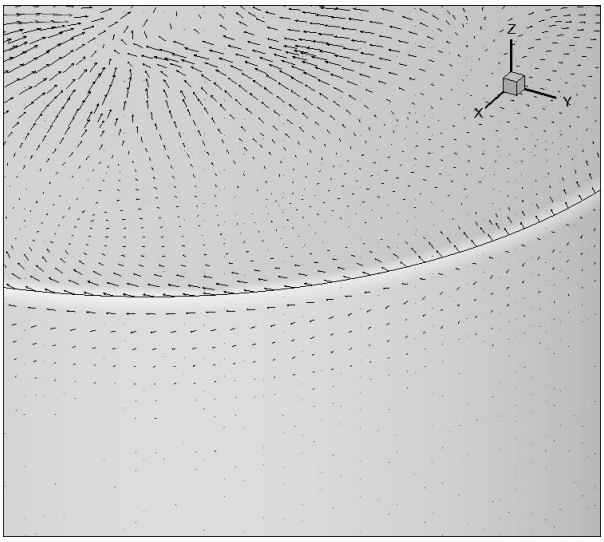

Figure 17 The vector map for the SPECT volume phantom at 0.1 second.

As stated in section 3.3.2, the air was phase1, water was phase2 and saline was phase 3. However, the TECPLOT 360 re-defined the phase name for some reasons, hence in TECPLOT image, air became phase2, water became phase3 and saline became phase4. An x-0 plane was created to help illustrate the volume fraction of saline at 0 seconds (shown in Figure 18). The 2cm air gap was simulated and air phase was also presented in Figure 18 (right), the air gap was contoured with red and the rest of phantom was blue. i.e. no air.

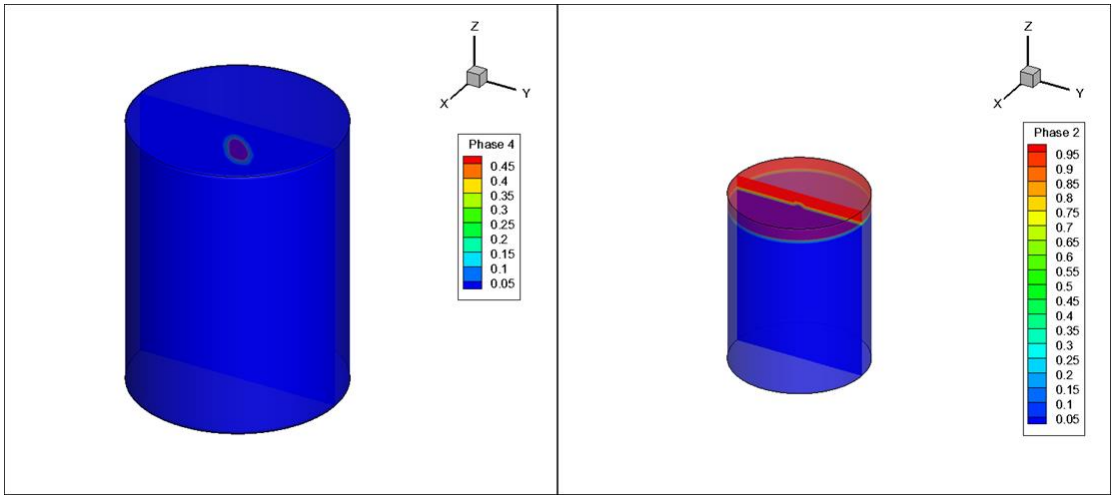

Figure 18 The volume fraction of saline phase on the x-0 plane (left) and the volume fraction of air phase (right) at 0 seconds.

The volume fraction of saline phase on the x-plane at 0.1 second is shown in Figure 19. It can be seen that the mixing process was fast and the saline solution was stretched to the wall of the phantom. In order to show the results more clearly, the isosurface for the volume fraction 0.15 was plotted, from which the flow trend of water and the mixing trend of radiopharmaceutical were validated.

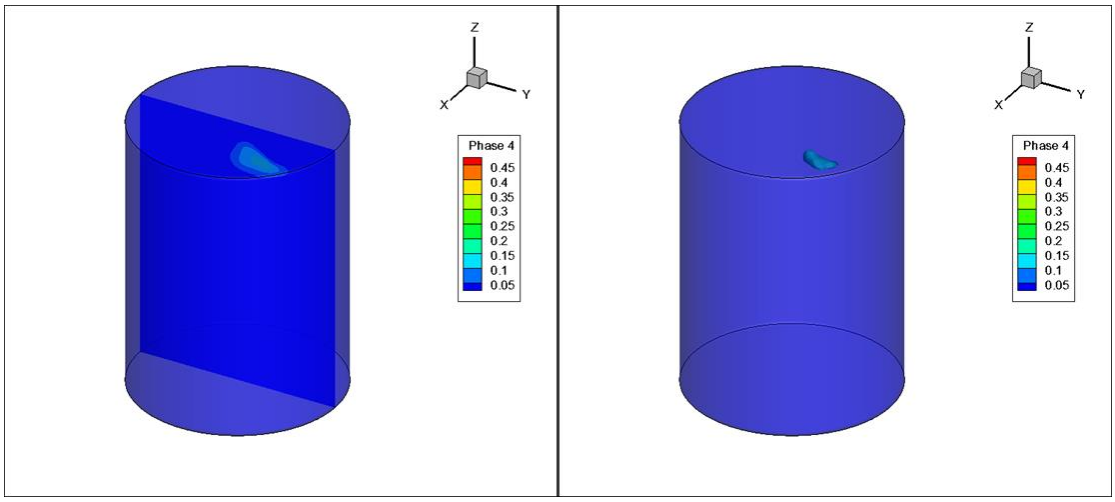

Figure 19 The volume fraction of saline phase on the x-plane (left) and the isosurface of saline phase at 0.1 second.

Shaking

In the user defined function 'shaking.c' (shown in appendix 2), the shake amplitude of the phantom was controlled by the movement velocity and movement time. The movement velocity was set to 0.3 m/s and the movement time was set to 1 second which started from 0.5 second after the beginning of simulation. i.e. the maximum displacement of the phantom was 0.3 metre from the origin. Hence, the mixing technique of shaking of the phantom was successfully simulated, as the phantom went up and down every second and the amplitude was 30 cm.

Result

The time step for this shaking simulation was 0.5 second and the iteration number for each step was 20, then some of simulated results at selected time were loaded to TECPLOT360 for further analysis.

The vector of each node at 0.5s and 1.5s on the phantom mesh is shown in Figure 20, where at 0.5s the phantom is moving up and at 1.5s the phantom is moving down.

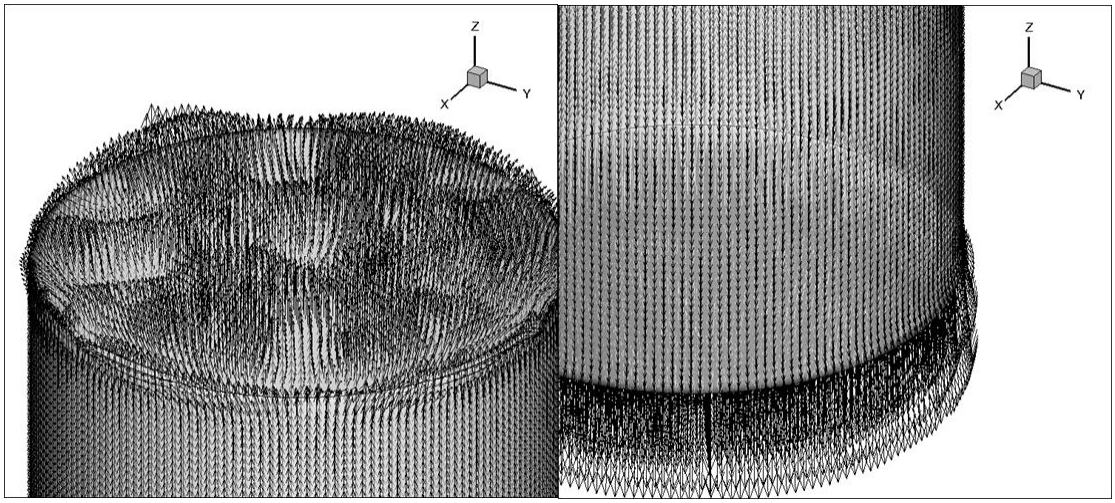

Figure 20 The vector map for the source tank phantom at 0.5 and 1.5 seconds.

Again the saline phase of 0.5s and 1.5s are shown in Figure 21. The mix technique of shaking was efficient and the volume of saline was disappeared by 1.5s. The two images in Figure 21 have been plotted in the same fraction scale. TECPLOT is just an image post processing tool, and was not ideal for illustrating the numerical changes in this simulation because it was not capable of showing any simulation result of saline volume fraction after 1 second.

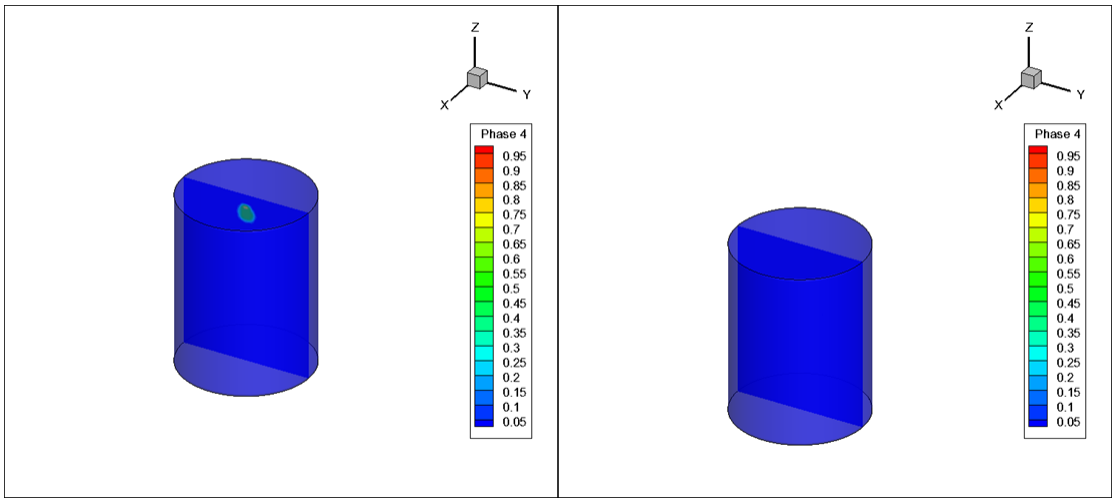

Figure 21 The volume fraction of saline phase on the x-0 plane (left) at 0.5 and 1.5 seconds.

Chapter4 SIMIND simulation and validation

4.1 Introduction

The purpose of this study was to build and validate the simulation model for SIEMENS E.Cam Dual-Detector Variable-Angle gamma camera. The SIMIND Monte Carlo package was introduced to simulate the imaging process of this gamma camera; also a series of experiments were performed to create and examine the validity of SIMIND model.

The experiments could be classified into two major parts: the first part was to measure and determine several key parameters for the input of the SIMIND simulation, since the parameters, such as energy resolution and intrinsic spatial resolution, were different for different types of gamma cameras and the value could vary with the age of gamma camera; the second part was to calibrate the inputs to SIMIND that may affect the performance of the simulation and validate the SIMIND simulation by applying correction factors and directly comparing the experimental and simulated results.

4.2 SIMIND SETTINGS

4.2.1 Simulation Platform and software version

The simulation platform was a SONY E series Laptop with Intel Core i5 Processor boosted to 3.10 GHz; the operating system was Windows® 7 Home Premium 64 bit.

The SIMIND package applied was Windows version 4.9 (Intel FORTRAN Professional compiler) 64 bit, which can be free downloaded from http://www2.msf.lu.se/simind/Downloads.html.

4.2.2 SIMIND settings

The SIMIND Monte Carlo package consists of two main programs: CHANGE and SIMIND. The CHANGE program is the user interface to define the simulated system and write the settings to external files. SIMIND performs the actual Monte Carlo simulation using input files generated by CHANGE and the simulation results are written to the screen and to different data files, such as an Interfile format file for images.

General Settings

In the general setting section of the CHANGE interface:

Sodium pertechnetate (Na TcO_4) with photon energy of 140.5 keV was the source in the experiments.

- Index1: Photon Energy: 140.5 keV.

The size of detector and crystal was determined from a Siemens data sheet, where the size of the crystal is 53.3 x 38.7 cm and the thickness of the crystal is 0.95 cm [8].

The inputs for CHANGE:

- Index 8: Crystal Half Length/ Radius: 29.550 cm.
- Index 9: Crystal Thickness: 0.95 cm.
- Index 10: Crystal Half Width: 22.250 cm

The structures, such as light guide and the photomultiplier tubes behind the scintillation crystal, were defined as equivalent to 4 cm Lucite [23].

- Index 11: Backscattering Material: 4 cm.

The NaI crystal was modelled as covered by 0.1 cm aluminium.

- Index 13: Thickness of Cover: 0.1 cm.

The solid angle for the photons was set to 1. This setting was called photon forcing, which could reduce the variance in SIMIND simulation and improves the detection efficiency by only generating and tracking photons within the geometry that have a chance of interacting with the crystal [24].

- Index 19: Photon Direction: 1.

The energy threshold was defined as 20 % and centred with the peak energy of the photon.

- Index 20: Upper Window Threshold: -20.
- Index 21: Lower Window Threshold: -20.

The intrinsic spatial resolution of the NaI crystal in the simulation must be determined by experiment, since this value was different for different gamma cameras and the value could vary as the NaI crystal aged. Thus, an experiment was performed to measure the intrinsic spatial resolution for the SIMIND simulation, which was covered as a part of spatial resolution validation experiment and the details were described in Section 4.7.

- Index 23: Intrinsic Resolution: 0.46 cm.

Energy resolution was the other key parameters that must be provided from experimental measurement, which was covered in the experiment of energy resolution validation and the details of the procedure are illustrated in Section 4.4.

- Index 24: Energy Resolution: 9.49 %.

The energy range in the SIMIND simulation was from 0 to 180 KeV, and there were 512 energy channels available; hence the energy value of each channel was 0.352 keV.

- Index 27: keV/Channel: 0.352.

The pixel size was determined from the data sheet of the E.Cam and was 0.48 for 128x128 images and 0.12 for 512x512 images.

- Index 28: Pixel Size in Simulated image: 0.48.

A low Energy High Resolution (LEHR) collimator was chosen for the imaging simulation, the LEHR collimator is typically used for Tc99m tomographic imaging [25]. The data for the Siemens LEHR collimator was listed in Chapter 2. Fortunately, SIEMENS Signature Series gamma cameras were popular in modern clinical application and scientific research, so the SIMIND package had a build-in dataset for the SIEMENS LEHR collimator, hence SE-LEHR collimator was used in the collimator parameters section.

- Index 46- 60: Collimator Parameters : *SE-LEHR

Simulation Flags

The panel of simulation flags is shown in Figure 22 for a planar acquisition. This consists of 15 flags to control various operational aspects of SIMIND. Several flags were very important in the SIMIND simulation of this study.

- Flag 4: Include the Collimator

  This flag controls the involvement of the collimator in the simulation. When the flag is set to be ‘TRUE’, the values of indices on Collimator Parameters page are incorporated into SIMIND.

- Flag 5: Simulate a SPECT Study

This flag initiates the SPECT simulation. i.e. the flag has to be set to be ‘FALSE’ for static planar imaging.

- Flag 7: Include Backscattering Material
- Flag 10: Include the Interactions in the Cover
- Flag 11: Include the Interactions in the phantom
- Flag 12: Include Simulation of Energy Resolution

In this study, the performance of Siemens E.Cam was simulated in almost every aspect; hence, these flags were set to be ‘TRUE’ for all simulations.

- Flag 14: Write File Header in INTERFILE V3.3 Format

This flag needs to be ‘TRUE’ for the data analysis in MATLAB, since the simulated results of SIMIND has to be imported to MATLAB using the ‘interfileread’ function.

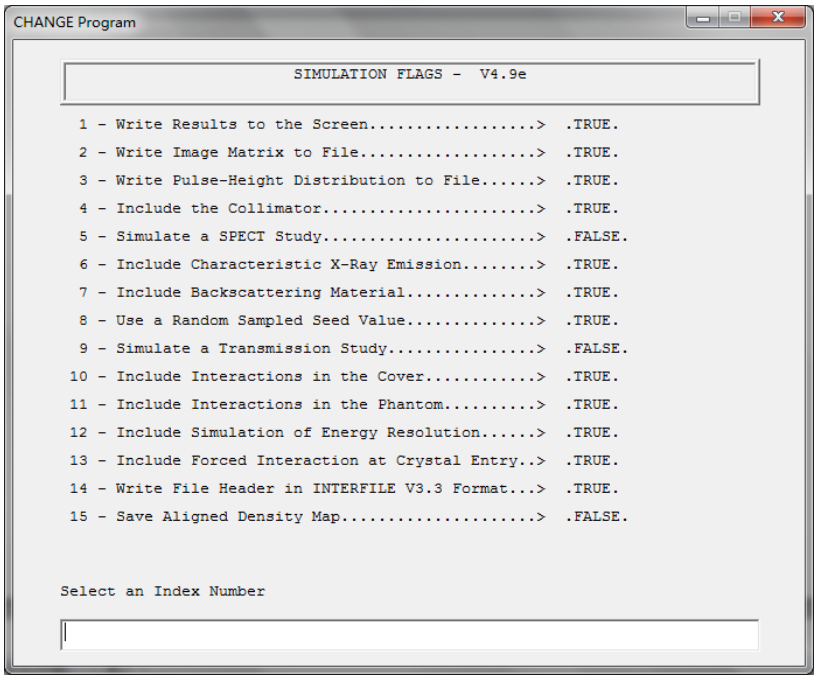

Figure 22 The SIMIND Simulation Flags panel in the setting of the CHANGE program.

4. 3 Background radiation measurement

During the scan process of the gamma camera, cosmic rays, natural radioactivity and surrounding shielding materials and other sources in the room are the sources of background radiation. For gamma cameras in hospitals, the patient who has been injected radionuclide could be an additional source of background radiation. Therefore, it is critical to make sure the background radiation to be kept as low as possible to minimize the statistical uncertainty [26].

The background radiation measurement of the Siemens E.Cam was performed before the start of any experiment. In this experiment, the detector 1 was set to 0 degree and detector 2 was set to 180 degree, also, the collimators of both detectors were removed; then a 5 minutes static acquisition was performed. The measured results were saved in a DICOM file, which was imported to MATLAB to display the image of background radiation. From the images from detector 1 and 2, the background radiation level was quite low, where the maximum count for both detectors was 5 (shown in Figure 23). Hence, the background radiation effect for the gamma camera in the Nuclear Medicine Department of Christchurch hospital could be neglected for the later experiments.

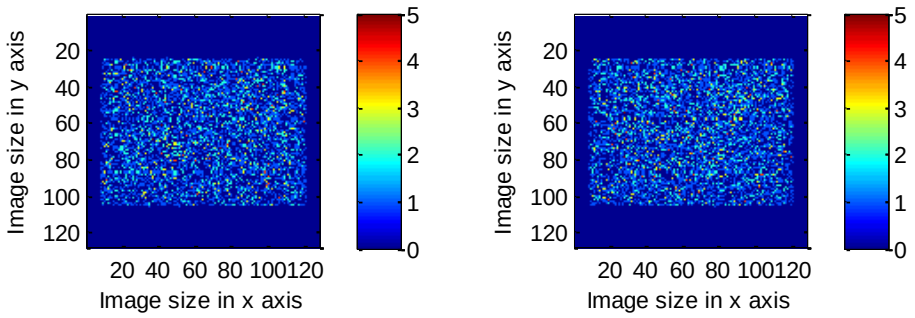

Figure 23 The background measurements of detector1 and detetctor2 for E.Cam gamma camera.

4. 4 Energy correction and validation

Instead of providing energy information of a spectrum directly, the output of Siemens E.Cam gamma camera delivers the binning number for each energy channel and the count number in the channel. In order to use the energy information in the further study, the energy spectra of two radioactive sources were investigated and a conversion or correction function of energy channel must be introduced.

4.4.1 Energy Spectrum

Experiment

In order to measure the energy spectra of Tc99m and Co57 source, the LEHR collimator was removed from both detectors and the spectrum acquisitions were set to record 50,000 counts at the photo-peak energy for each radioactive source.

- Tc99m spectrum

A 3ml Syringe containing 0.2ml NaTc99m was placed 1 meter above the floor and 2 meters away from the detectors of E.Cam. The activity of the Tc-99m source was 11.54 MBq. The phantom and detector arrangement are shown in Figure 24.

- Co57 spectrum

The Co57 source was placed at the same position of Tc99m source, which was one meter above the floor and two meters away from the detectors.

Figure 24 The experiment arrangement of detector and source for Tc99m.

Simulation

The acquisition of the Tc99m spectrum was simulated using the SIMIND package.

The volume of 0.2 ml NaTc99m contained in the syringe was not a perfect cylinder; hence the source was simulated as a spherical source to increase the accuracy of the simulation:

$$V = \frac{4}{3}\pi r^3 \text{ , where } V=0.2ml$$

From the equation above, the radius of the point source r = 0.363cm.

The collimation flag was set to be turn off at the simulation flag section.

- Flag 4: Include collimator: FALSE.

Results

After the acquisition, the measured data for Tc99m and Co57 were recorded by the Siemens E.Cam software. Three of the key results are summarized in Table 6 listed below. From Table 6, the peak energies for Tc99m and Co57 were exactly the same as specified: 140.5 KeV and 122.1 KeV.

DETECTOR1	
Tc99m	**Co57**
Peak energy: 140.5 KeV	Peak energy: 122.1KeV
Peak Channel: 1015.15 Channels	Peak Channel: 892.347 Channels
Energy Resolution – FWHM: 9.48961%	Energy Resolution – FWHM: 10.604%
DETECTOR2	
Tc99m	**Co57**
Peak energy: 140.5 KeV	Peak energy: 122.1KeV
Peak Channel: 1015.44 Channels	Peak Channel: 892.17Channels
Energy Resolution – FWHM: 9.96929%	Energy Resolution – FWHM: 10.1702%

Table 6 The measured results of Tc99m and Co57 in Detector1 and Detector2.

4.4.2 Energy calibration function

The peak energy and peak channel could be used to determine the energy per channel for Siemens E.Cam instead of the binning numbers. The energy calibration factors could be calculated from:

Peak Energy = Factor (a)*Peak Channels +Factor (b)

From the measurements of peak energy and peak channel for Tc99m and Co57 in detector1:

140.5 = 1015.15* Factor (a) + Factor (b)

122.1 = 892.347 * Factor (a) + Factor (b)

Thus, solve the two equations:

Factor (a) = 0.1498

Factor (b) = -11.57

The energy calibration function is:

Energy = 0.1498*Channels -11.57.

This energy calibration factor must be applied to the energy spectrum extracted from the Siemens E.Cam to convert bin number to energy value.

4.4.3 Energy spectrum validation

In order to plot the energy spectra of Tc99m and Co57, the detector1 images of the E.Cam gamma camera were imported into MATLAB by 'dicomread' function. The information of binning number and counts was extracted from the DICOM file, and then the energy correction was applied to create the energy data set. Also, the count number for each energy section was normalized by the maximum count. The spectra of Tc99m and Co57 (shown in Figure 25) were plotted by the MATLAB code. The data processing and plotting procedures are summarized in MATLAB 'Tc99m_Co57.m' (Appendix 3).

The acquisition progress of Tc99m energy spectrum was simulated in SIMIND Monte Carlo Simulation. The normalized Tc99m energy spectra from E.Cam measurement and SIMIND simulation are plotted in Figure 26. There was good agreement between the measured and simulated photo peaks. The MATLAB code for this analysis is illustrated in 'EnergyResolutionECAMvsSIMIND.m' in Appendix 4.

However, the measured result (blue curve) had some additional scatter near 100 KeV, which was caused by the backscattering effect from the gamma camera itself and the scatter from surrounding environment. In fact, the backscattering effect was considered before the simulation, the difference was still significant. This is one of the limitations of SIMIND package, the backscattering simulation was not very accurate, since the materials in the gamma camera were directly related to the machine design (i.e. the simulation must be different for different gamma camera) and there was not much research focused on the accurate simulation of backscattering. Better approximation and validation experiment were the next approach to improve this part of the simulation.

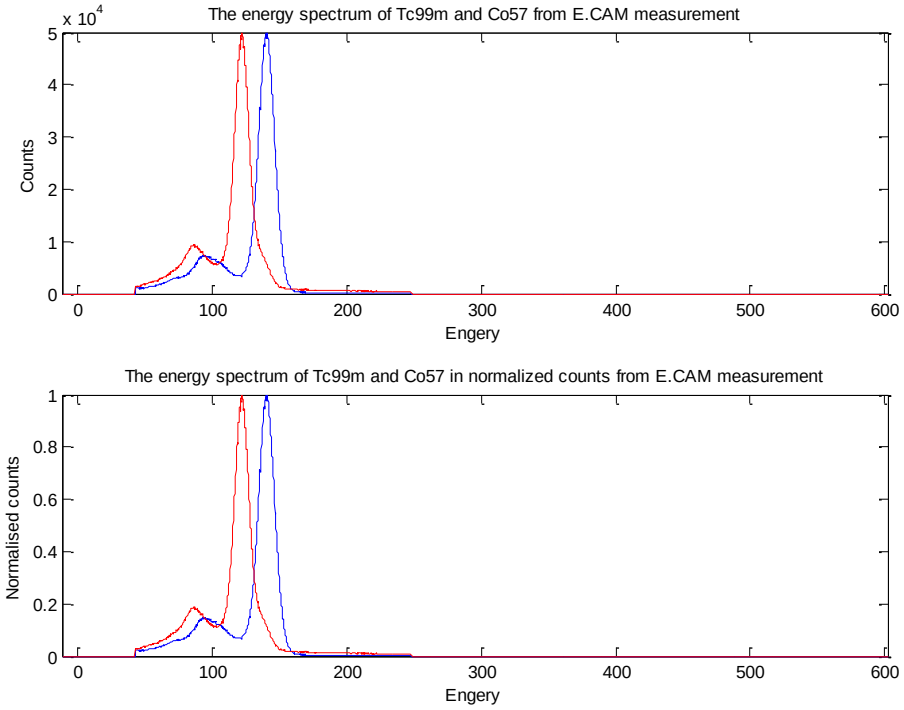

Figure 25 Corrected energy spectra of 50,000 counts (Top) and normalized counts (Bottom) for detector1, while the blue curve indicates the spectrum of Tc99m and the red curve indicates the spectrum of Co57.

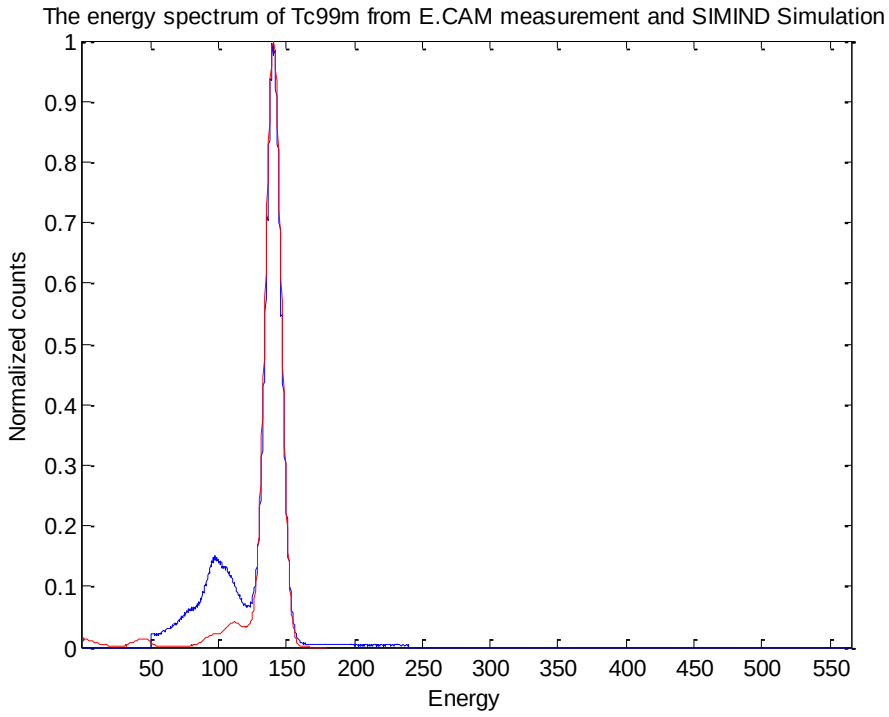

Figure 26 Corrected Tc99m energy spectra in normalized counts from the E.Cam measurement (Blue) and SIMIND simulation (Red) were overlaid together.

4. 5 Bed attenuation correction

The Siemens E.Cam is a dual-detector gamma camera; there is a bed that holds patient during the image acquisition. Even though the bed is made of a low density material, such as Aluminium, the attenuation effect of the bed can still affect the accuracy of the scan. Therefore, an attenuation correction factor must be determined for further use in the study.

Experiment

The radiopharmaceutical used in this experiment was Tc-99m in saline solution, the activity of the source was 95.1MBq; after injecting the solution into the IEC insert phantom, and the residual activity was 0.13 MBq. Hence, the activity of the Tc-99m inside the phantom was 94.97 MBq.

Detector 1 was set to 0 degree and Detector 2 was set to 180 degree, the radius was 7.0 cm and 13.4 cm respectively (i.e. the distance between detector1 and dector2 was 20.4cm). The IEC phantom was placed 10 cm above detector 2.

- With Bed

  The patient bed was insert between the IEC phantom and detector 1(as shown in Figure 27), the distance from detector 2 to the bottom of patient bed was 12.5 cm.

- Without Bed

  The patient bed was removed and the position of IEC phantom was remained unchanged (as shown in Figure 28).

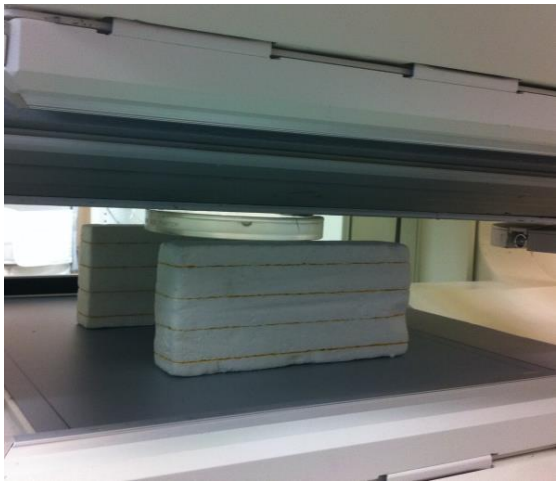

Figure 27 The experiment setup of detectors and IEC insert phantom with patient bed.

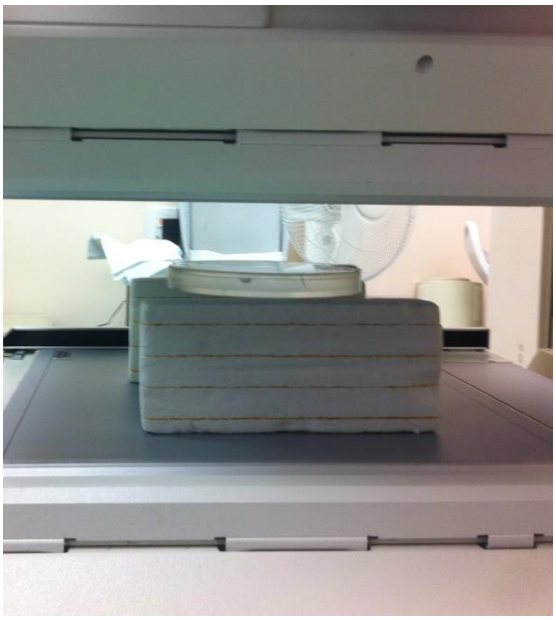

Figure 28 The experiment setup of detectors and IEC insert phantom without bed.

Two 5 minutes static acquisitions were performed: one with the patient bed and one without patient bed. The images were saved in DICOM file and circular ROI was defined manually along the image edge of IEC phantom in ImageJ.

Result:

With Bed:

For detector 1, the total counts were 2301646; and the ROI counts were 2057919.

For detector 2, the total counts were 2310419; and the ROI counts were 2247142.

Without Bed:

For detector 1, the total counts were 2283782; and the ROI counts were 2205172.

For detector 2, the total counts were 2251528; and the ROI counts were 2210414.

For detector 2, there was nothing between the phantom and detector 2 for both acquisitions, the counts with bed was slightly higher than the counts without the bed. The difference was reasonable and caused by the decay of the radiopharmaceutical. However, for detector1, the attenuation effect of patient bed is not negligible. The bed attenuation factor for detect 1 could be calculated by:

$Detector1\ count\ with\ bed\ /_{Detector1\ count\ without\ bed} = {}^{2057919}/_{2205172} = 0.933 \pm 0.016$. This correction factor must be considered for further simulation and experiment of detector 1 to improve the accuracy.

4. 6 Sensitivity validation

The sensitivity measures the counts per second per unit activity, which is one of the key measurements in quality assurance for gamma cameras. This experiment was to examine the sensitivity of the Siemens E.Cam and validate the simulated result.

Experiment

The experimental data of bed attenuation (in section 4.4) could be used to determine the sensitivity of E.Cam. Thus, the data of detector1 scan without the patient bed was chosen to confirm stability of the sensitivity during the series of experiments. The images of the IEC insert phantom from detetor1 and detector 2 were plotted in Figure 29.

For detector 1, the total counts were 2283782; and the ROI counts were 2205172. The activity of Tc99m source was 94.97 MBq and the acquisition time was 5 minutes, which was 300 seconds.

Hence, the sensitivity for detector1 = ROI counts / acquisition time / activity
= 2205172/ 300/ 94.97
= 77.399 [cps/MBq]

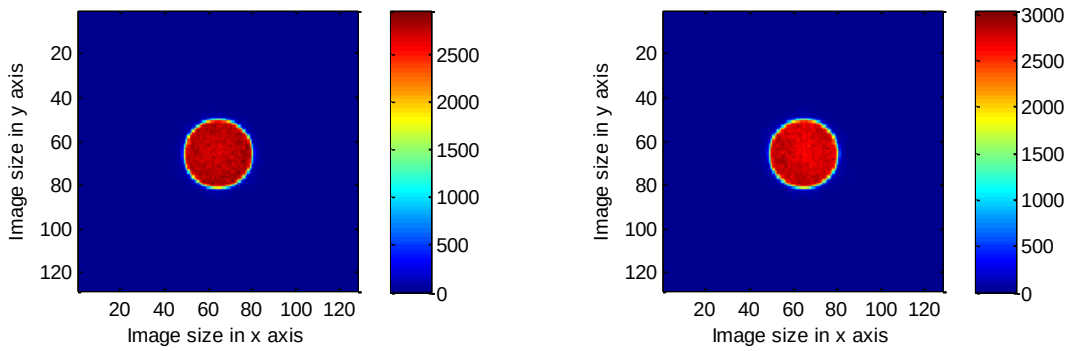

Figure 29 The images of sensitivity measurement from detector 1 (left) and 2 (right).

Simulation

The dimensions of the IEC insert and the inner volume were set to the index 2 to 7, where the radius of the phantom was 8.5 cm and the thickness was 2 cm; radius of the source (inner volume of the phantom) was 7.5 cm and the thickness was 1cm. The image size was set to 128x 128. SIMIND was set to simulate 10 million photon histories.

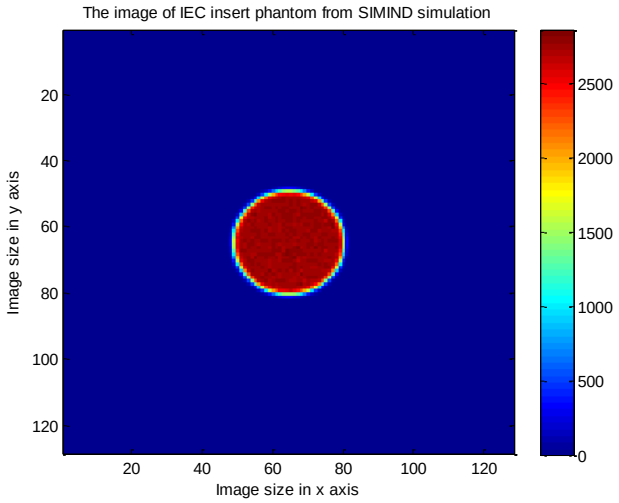

Figure 30 the images of sensitivity measurement from the SIMIND simulation.

The output image from the SIMIND simulation is shown in Figure 30.The simulated results of SIMIND, including sensitivity value, were saved in the output file with extension name of 'res'. The sensitivity of the simulated E.Cam model was 75.3174 cps/MBq.

Analysis

There was a small variation in the sensitivities from E.Cam measurement and simulation. The variation might be caused by the counts of scattered photons from

the gamma camera head, floor and walls etc., and SIMIND could not simulate these complex circumstances and count the scattered photons. However, the difference between experimental and simulated results was 2.689%, which was acceptable in terms of accuracy.

4. 7 Spatial resolution validation

The validation of spatial resolution was the final part of the validation experiment series. The line Spread Function (LSF) and Full Width Half Maximum (FWHM) values were determined from the measurement of simulated line source.

Experiment

The Nuclear Associates line source phantom was used in the experiment for spatial resolution validation. The length of the phantom is 23 cm and the diameter is 1.28±0.01 cm; the length of the source (inner tube) is 22 cm and the diameter is 1.18±0.01 cm.

The radiopharmaceutical used in this experiment was Tc-99m in saline solution, the activity of the source was 257MBq; after injecting the solution into the line source phantom the residual activity was 107.4 MBq. Hence, the activity of the Tc-99m inside the phantom was 149.6 MBq.

The phantom was placed 10 cm above the collimator of detector2 and also set the distance between the source centre and the collimator of detector1 was set to 10 cm. Detector1 and detector2 were set face-to-face, i.e. detector1 at 0 degree and detector2 was at 180 degree. The phantom and camera arrangement are shown in Figure 31. The other phantom and camera arrangement in this experiment was changing the source

centre-to-collimator distance to 23.5 cm for both detectors. Further static images of the line source phantom were acquired for 5 minutes with the source-to-collimator distance of 23.5cm.

Figure 31 The experiment setup of line source phantom and detectors, where the distance of source centre to collimator of both detectors was 10 cm.

The images of the line source phantom from the E.Cam gamma camera were saved in the DICOM file format and imported into MATLAB for analysis. The image information was read by the 'dicomread' function and the images of the line source phantom were plotted by MATLAB code 'LineprofileT2.m' (Appendix 5):

For the arrangement of source centre to collimator of 10 cm:

The image of detector1 is shown in Figure 32 (a);

The image of detector2 is shown in Figure 32 (b).

For the arrangement of source centre to collimator of 23.5 cm:

The image of detector1 is shown in Figure 33 (a);

The image of detector2 is shown in Figure 33 (b).

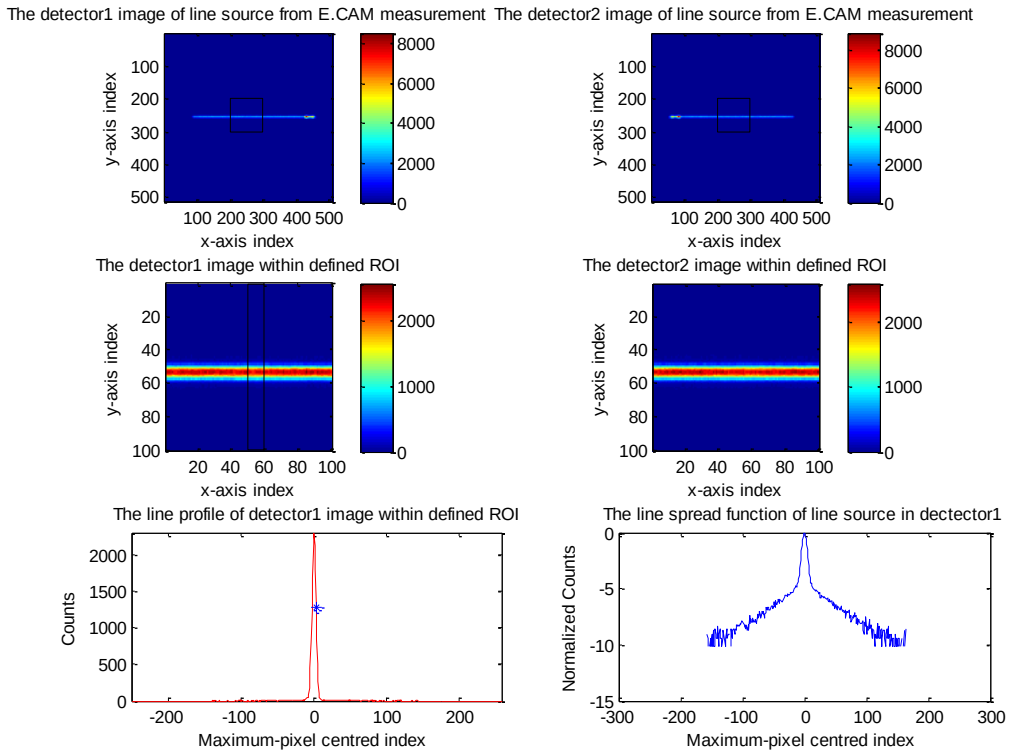

Figure 32 The experiment results for the setup of the source centre to collimator was 10 cm, where

a) The detector 1 image of the line source phantom
b) The detector 2 image of the line source phantom
c) The detector 1 image of the line source phantom within defined ROI
d) The detector 2 image of the line source phantom within defined ROI
e) The line profile of detector1 image within the defined ROI
f) The line spread function of the line source in detector1.

A ROI of 100x100 pixels, which is outlined by the black square on Figure 32 (a) and Figure 33 (a), was defined to examine the spatial resolution of the line source phantom. The detector1 image within the selected ROI was plotted in Figure 32(c) and Figure 33 (c); then another ROI of 10x 100 pixels was defined from the centre of the image, where the values of the 10 indices were averaged to plot the line profile of

the line source phantom. The indices of the image were re-arranged to centre about the maximum pixel index. The counts for each pixel were normalized to the maximum value, then the line profile of detector1 images were plotted in Figure 32 (e) and Figure 33 (e) respectively. Also, the index of the geometric centre (‘blue star’) was marked on the plot of the line profile.

The index of the pixel with maximum counts and the index of the geometric centre were not the same for both arrangements; however, the index of geometric centre in the 10cm arrangement in Figure 32 (e) was closer to the index of the pixel with maximum counts compared with that of the 23.5 cm arrangement in Figure 33 (e).

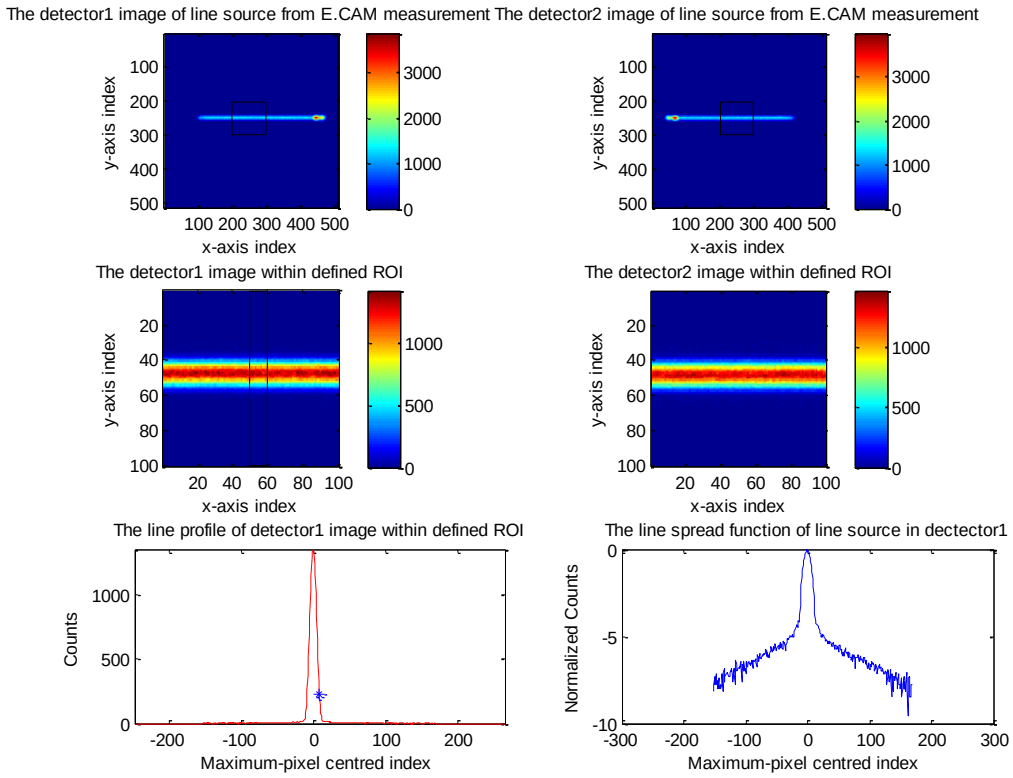

Figure 33 The experiment results for the setup of the source centre to collimator was 23.5 cm, where

a) The detector 1 image of the line source phantom
b) The detector 2 image of the line source phantom
c) The detector 1 image of the line source phantom within defined ROI
d) The detector 2 image of the line source phantom within defined ROI
e) The line profile of detector1 image within the defined ROI
f) The line spread function of the line source in detector1.

Simulation

Followed similar procedures, the line profile for the SIMIND simulation is plotted in Figure 34. As expected, the index of the geometric centre (‘blue star’) was right on the peak of the profile, which means the index of the pixel with maximum counts and index of the geometric centre were the same. The simulation of SIMIND was performed in ideal conditions and that may not completely represent the experimental

measurement. For example, in the SIMIND simulation the position of the line source phantom could be defined in the centre of the FOV of gamma camera; in the experimental setup the position of the line source phantom had to be aligned manually. Any small displacement of the phantom could change the index of maximum pixel directly.

When the two normalized line profiles that from E.Cam and SIMIND were plotted together the agreement was very good (shown in Figure 35). This plotting was performed by the MATLAB code 'LineProfileComp.m' in Appendix 6. Finally, the line spread functions for the image of the experimental scan and the Monte Carlo simulation (in Figure 36) were plotted using the MATLAB code 'LineSpredFunctionComp.m' in Appendix 7.

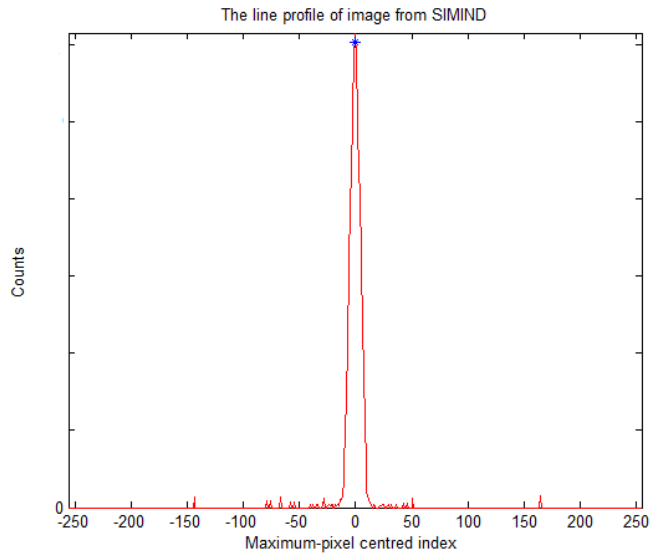

Figure 34 The simulated line profile (red) that centred with the index of pixel with maximum count, the geometric centre was marked as blue star *.

The central part of those two line spread function were perfectly overlaid on each other. There were large variances in the pixel counts from the SIMIND simulation

when moving away from the central part of the line spread function; hence some refinements are still required for this model. The FWHM value for the spatial resolution could be measured on the line spread function; fortunately, the FWHM section was on the overlaid part (i.e. same FWHM). From the direct measurement, the spatial resolution in FWHM was approximately 9.55%. The spatial resolution measurement successfully validated the SIMIND simulation of the line source.

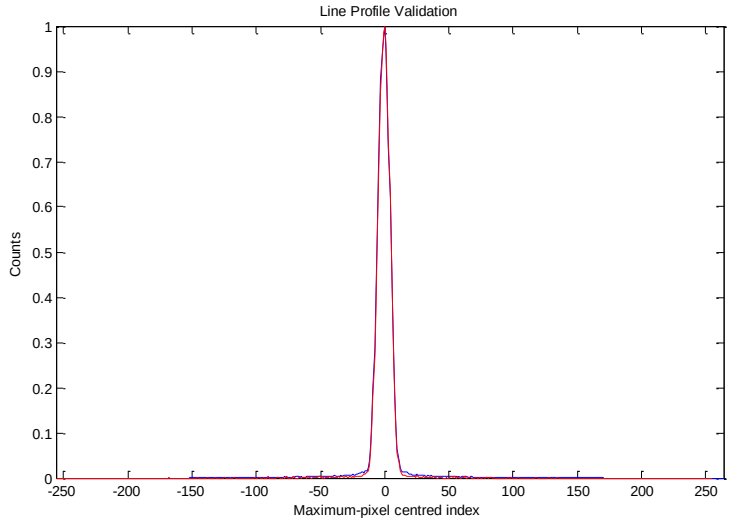

Figure 35 The simulated (red) and the measured (blue) line profile centred with the index of the pixel with the maximum counts.

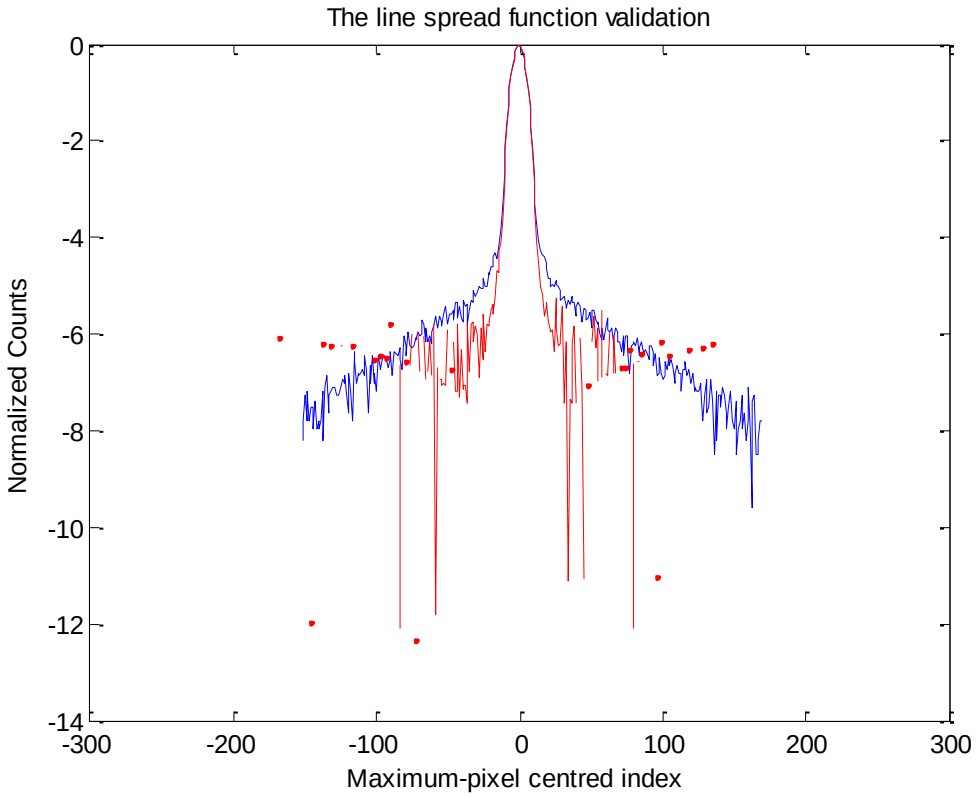

Figure 36 The simulated (red) and the measured (blue) line spread function that centred with the index of the pixel with the maximum counts.

Chapter5 Volume simulation and reconstruction

The basis behind the simulation is that the degree of mixing that is required will be dictated by the impact that the acquisition and reconstruction have on the image quality, this being image uniformity for the case of the uniform volume phantom. Small patches of non-uniform mixing may be present in the fluid dynamics output, but the impact of spatial resolution and noise could mean that these are of little significance in the tomographic images. This requires Monte Carlo simulation to generate a set of planar projections, then reconstruction of these projections using, for example, filtered backprojection to generate tomographic slices that can be assessed for image uniformity. Because computing limitations meant it was not possible to run a full 3D simulation of the fluid mixing to a point of apparent uniform concentration (as seen with the FLUENT output), a snapshot of the mixing at 0.1 seconds into the FLUENT simulation was used to test if a combination of fluid dynamics and Monte Carlo simulation of imaging could be performed. This was considered a proof-of-concept experiment. The 3D simulation was selected from the FLUENT simulation result 'Rotation 4-1-00001.dat'.

The concentrations for the radiopharmaceutical were exported from FLUENT as node data and imported into MATLAB. The node data was converted to a spatial mesh using

the MATLAB 'griddate3' function which uses the Delaunay triangulation of the data based on the QuickHull algorithm [27].(Appendix 9)

A 64 projection SPECT simulation was run to generate 64x64 images with approximately 600k counts per projection simulated. Ignoring attenuation by the phantom, 370 MBq in the cylindrical volume of 23 cm diameter and 31 cm long will give a count rate at the Siemens E.Cam detectors of approximately 370 MBq x 91 CPS/MBq = 33.6k CPS using the published sensitivity specification for a Siemens E.Cam detector with low energy high resolution (LEHR) collimators. For a typical quality control SPECT acquisition of 20 seconds per projection, the total counts incident on the detector would be approximate 673k counts. In a practical situation the total counts would be much less than this because of the attenuation of the water filled phantom. The detailed SIMIND input is listed in Appendix 8.

The SIMIND source map (in this case the activity concentration exported from Fluent and post-processed in MATLAB) was used to determine the photons simulated. The total photons per projection were simulated using this source map (equivalent to the sum of all the integer values in the source map). The source attenuation coefficients were simulated geometrically using a horizontal cylindrical phantom of the same dimensions as the cylinder used in Fluent to generate the source map. The resulting volume data was scaled to give a simulation with photons per projection of approximately 600 K.

The simulation generated a set of real valued projection data. This data set was imported into MATLAB and reconstructed using the inverse Radon transform in the MATLAB Image Processing Toolbox. The reconstruction was performed using cubic interpolation and a Hamming filter set with a cut-off at the Nyquist frequency. (Appendix 10)

A series of sample transaxial slices through the reconstruction are shown in Figure 37. A comparison of the projection data and slice image of 47 demonstrated the success in simulation and reconstruction and the feasibility of the combined simulation concept in this study.

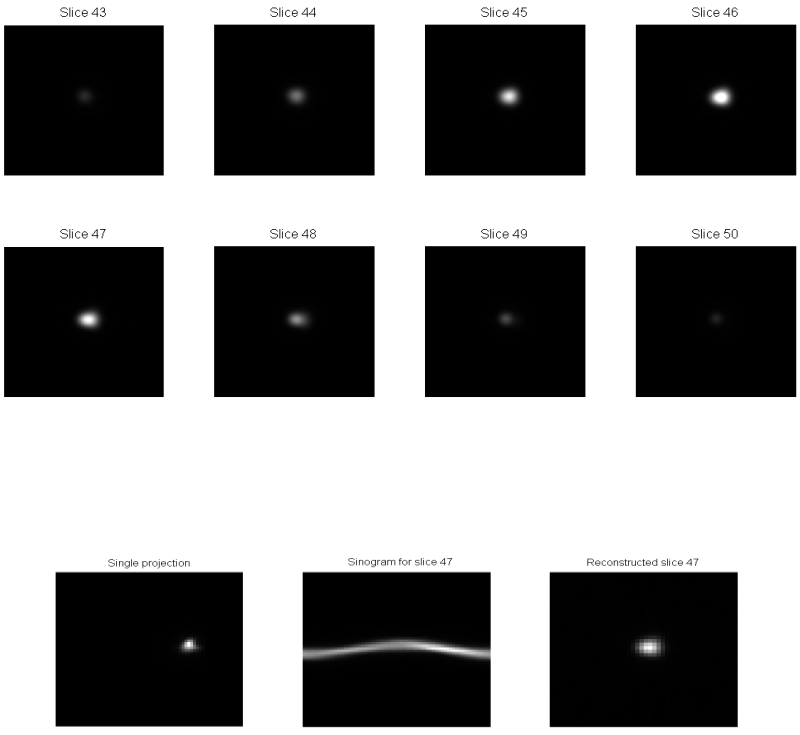

Figure 37 Sample transaxial slices through the reconstruction, and a comparison of the projection data and slice image.

Chapter 6 Discussion and future work

6.1 Discussion

6.1.1 FLUENT simulation

Firstly, the FLUENT simulation of the mixing process was successful. Both the results for the spinning and shaking simulations were reasonable and provided the water flow and mix trends for later analysis. However, the simulation for the mixing of TcO_4 was not achievable due to the lack of key parameters and reference.

Secondly, the computation time was also critical for this study. A 3D FLUENT simulation took around 10 days to finish and this made refining and adjusting the simulation difficulty. The mesh quality had to be reduced intentionally to reduce the simulation time. Hence, the computational resource is a key component for the FLUENT simulation in this study and further optimisation and computer resources will be required for a more extensive simulation.

Thirdly, there are several other models that could be used to simulate the phantom mixing action. The Eulerian-Eulerian three-phase mixture was a fast approach; the accuracy of the simulation could possibly be improved by applying another model.

6.1.2 SIMIND simulation

Firstly, the investigation of SIMIND simulation was helped by SIMIND being a well-studied package and a lot of research had been done by using this package; also,

there are many articles related to the construction of gamma camera models and the simulation of image acquisition.

Secondly, the SIMIND model is not perfect. Although it can simulate the performance of Siemens E.Cam gamma camera efficiently, some details in the simulation are not ideal. For example, the difference of measured and simulated energy spectrum due to scattering was significant, and although not considered significant in this study, further corrections process would be necessary for a more accurate simulation. Also if the detector setup is changed, the correction procedure for SIMIND simulation will need to be repeated.

Thirdly, during the work of this project the GATE (Geant4 Application for Tomographic Emission) package was also considered. GATE has many advantages compared with SIMIND; the most important one is it allows time-dependent simulation, such as detector movements and source decay kinetics. Hence, GATE could be used to simulate more realistic acquisition conditions [11].

6.1.3 Volume reconstruction

The successful volume reconstruction proved the concept of this study: FLUENT and SIMIND could be linked together to investigate the techniques of phantom mixing. i.e. The phantom mixing techniques, procedures and results could be simulated by FLUENT, and the related gamma camera image acquisition could be simulated by SIMIND which makes the investigation of phantom mixing become pure virtual.

6.1.4 Entropy analysis

The aim of this research was to optimise the quality control procedure to reduce unnecessary radiation exposure of clinical staff; hence all the work was focused on creating and examining proper mixing techniques. But how to determine if the phantom is well mixed is a potential problem for this research.

If the radiopharmaceutical in the phantom is poorly mixed, the clinical staffs have no chance to spot the problem until the start of scan. The uniformity of a gamma camera tomographic image could be tested by applying integral uniformity index or differential uniformity index etc. Is there any numerical index or method that could be used to define the level of mixing? The entropy measurement might be the tool to solve this problem.

Entropy means the degree of randomness of a system, where high entropy indicates high degree of randomness and low entropy indicates a low degree of randomness. The disadvantage of the entropy measurement was it could not give spatial information. However, the spatial information might not be crucial for this study, since all we need to know is whether the radiopharmaceutical in the phantom is well mixed instead of where or which area it is not well mixed. In fact, the entropy method has been used for the analysis in stratospheric dynamics for many years [28].

A few simple FLUNT simulations (2D roll simulation) were performed to examine the idea of entropy measurement. A series of saline mixing data was selected and then

imported into MATLAB. The series of images were plotted with contour lines, then the entropy for each image was plotted against time (Figure 38). The trend of the entropy value matched the mixing progress:

- When the mixing began, the entropy was high but was not at the maximum value, since the radiopharmaceutical had not dispersed completely yet.
- A few seconds later, the entropy reached the peak value. i.e. the randomness of radiopharmaceutical distribution reached a maximum through the mixing action.
- Then the entropy value began to drop with the uniform distribution of the radiopharmaceutical, and dropping to 0 at the end of the simulation.
- In addition, the contour line values on each image were different; in the last image the contour line values on the image were almost the same.

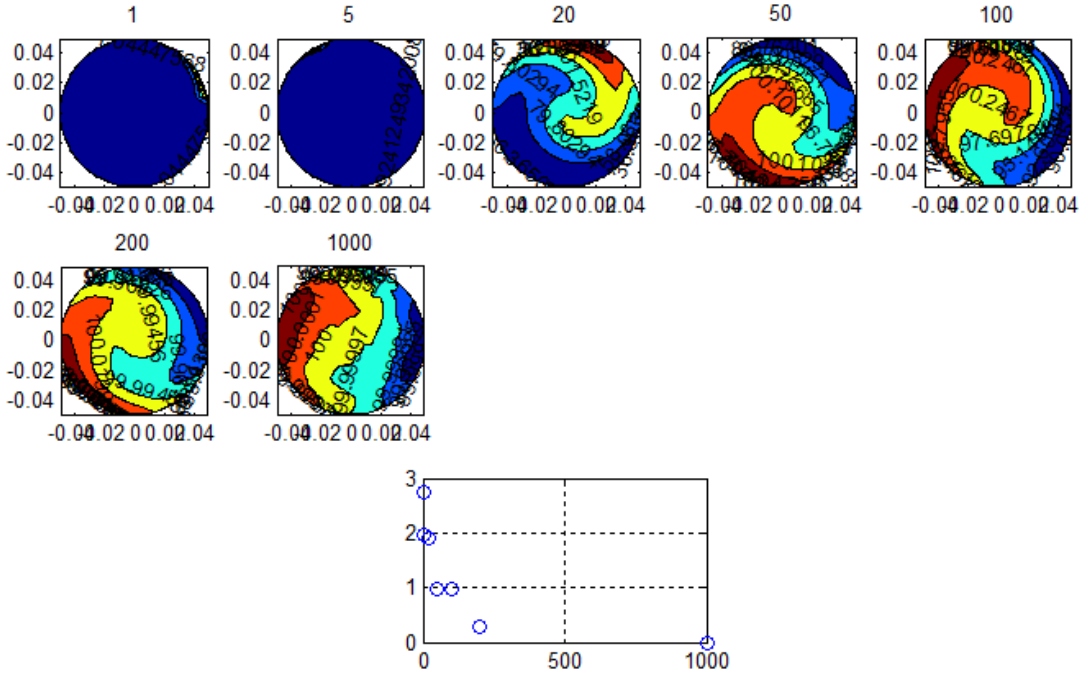

Figure 38 Simulated images of simplified rolling of the phantom and entropy values against image index (which is the time, the time step for each index is 0.1s).

6.2 Further work

6.2.1 FLUENT simulation

The three assumptions of uniform distribution of TcO_4- in the solution, similar molecule sizes between $NaTcO_4$ and NaCl and no heat transfer during the mixing process were the basis of the current FLUENT simulation in this study. More experiments and investigations could be made to examine the properties of sodium pertechnetate (Na TcO_4), such as viscosity, to simulate the real distribution of TcO_4-. Also, more work could be done to fine tune FLUENT simulation; hence the more realistic simulation that involves heat transfer could be performed. Instead of simulating the source tank, the simulation of phantoms with complex inserts could be attempted. In addition, the mixing techniques simulated in this study were simplistic. FLUENT is capable of more complicated phantom movements; more mixing techniques could be simulated in future research.

6.2.2 Entropy analysis

In the future, the entropy theory could be investigated in detail and its measurement could be extended to the real phantoms. Furthermore, proper entropy reference values for mixing different phantoms could be developed, leading to specific instructions on the phantom preparation for clinical staff and will hopefully result in unnecessary radiation exposure being significantly reduced.

Chapter 7 Conclusions

The aim of this study was to optimize the procedure in quality control testing to reduce the unnecessary radiation exposure to clinical staff. The investigation of phantom mixing was chosen because it was thought that efficient phantom mixing would mean less time needed to handle radioactive materials and less harm to people.

Firstly, the theory of fluid dynamic models for mixing was studied and a Eulerian-Eulerian three-phase mixture model was chosen to simulate the phantom mixture problem. By applying a user defined function, the mixing techniques of spinning and shaking were successfully simulated using FLUENT. Secondly, the characteristics of the Siemens E.Cam gamma camera were simulated by the Monte Carlo package SIMIND. The performance of the simulated gamma camera model was validated by a series of experiments, where the agreement between experimental and simulated results was demonstrated. Thirdly, the simulated phantom mixing data from FLUENT was used as the SIMIND source model and the successful volume reconstruction completed the overall simulation and verified the concept of this research.

Overall, FLUENT and SIMIND can be used together to study the phantom mixing problem to reduce the safety concern in the quality control test, where FLUENT is used to simulate the mixing process, SIMIND is used to examine the results.

Reference

1. **Iniewski, K.,** ***MEDICAL IMAGING: Principles, Detectors, and Electronics*****2009: Wiley-Interscience.**

2. **Webb, A.R.,** ***Introduction to biomedical imaging*****2003, New York;Chichester Wiley.**

3. **Kuwert, T.** ***SPECT-CT versus PET-CT*****. 2006; Available from: http://www.european-hospital.com/en/article/337-SPECT-CT_versus_PET-CT.html.**

4. **Wang, R.,** ***Fundamentals of medical imaging: Edited by Paul Suetens, Cambridge University Press, 2002, 280 pp. ISBN 0521803624, 70 GBP, 100 USD.*** **Biosensors and Bioelectronics, 2003. 18(7): p. 961-962.**

5. **White, S.** ***TU-B-201C-01: Gamma Camera and SPECT Routine Quality Assurance Testing*****. 2010. AAPM.**

6. **Siemens,** ***MEDISOFT Mixer Trolley Systems,*** **2011.**

7. **O'Connor, M.K.,** ***Quality Control of Scintillation Cameras (Planar and SPECT).***

8. **Siemens Medical Solutions USA, I.,** ***Siemens e.cam Signature Series,*** **2002.**

9. **MT Bahreyni Toossi, J.P.I., M Momennezhad, M Ljungberg, SH Naseri,** ***SIMIND Monte Carlo simulation of a single photon emission CT.*** **Journal of Medical Physics, 2010. 35(1): p. 42-47.**

10. **Loudos, G.K.,** ***Monte Carlo simulations in Nuclear Medicine.*** **AIP Conference Proceedings, 2007. 958(1): p. 147-150.**

11. **Buvat, I. and D. Lazaro,** ***Monte Carlo simulations in emission tomography and GATE: An overview.*** **Nuclear Instruments and Methods in Physics Research Section A: Accelerators, Spectrometers, Detectors and Associated Equipment, 2006. 569(2): p. 323-329.**

12. **Ljungberg, M.,** ***The SIMIND Monte Carlo program.*** **1997.**

13. **National Institutes of Health.** ***ImageJ*** **22 July 2013; Available from: http://rsbweb.nih.gov/ij/index.html.**

14. **Fluke Corporation, *Nuclear Associates 76-826 Spatial Resolution Phantom for SPECT Systems.* 2005.**

15. **National Electrical Manufacturers Association, *NEMA: Standards Publication NU 1-2001: Performance Measurements of Scintillation Cameras.* 2001.**

16. **Fluke Corporation, *Nuclear Associates 76-823,76-824, 76-825 PET/ SPECT Phantom Source Tank, Phantom Insert and Cardiac Insert*, 2005: USA.**

17. **Bakker, E.M.M.a.A., *Computational Fluid Mixing.* Handbook on Mixing, 2001.**

18. **Datta, R. and S.A. Vilekar, *The continuum mechanical theory of multicomponent diffusion in fluid mixtures.* Chemical Engineering Science, 2010. 65(22): p. 5976-5989.**

19. **FluentInc., *FLUENT 6.3 User's Guide.* 2006.**

20. **University of Canterbury, *About BlueFern*. Available from: http://www.bluefern.canterbury.ac.nz/about/.**

21. **Company, B.D.a. *BD Product Catalog*. 2013; Available from: http://catalog.bd.com/bdCat/viewProduct.doCustomer?productNumber=309628 .**

22. **WindSim. *What are the residuals?* 2012; Available from: http://user.windsim.com/index.php?action=artikel&cat=14&id=48&artlang=en.**

23. **Ljungberg, M., A. Larsson, and L. Johansson, *A new collimator Simulation in SIMIND based on the delta-scattering technique.* Nuclear Science, IEEE Transactions on, 2005. 52(5): p. 1370-1375.**

24. **Ljungberg, M., *The SIMIND Monte Carlo program*, 1989.**

25. **Inoue Y, S.I., Machida T, Yoshizawa Y, Akita F, Doi I, Watadani T, Noda M, Yoshikawa K, Ohtomo K., *Physical characteristics of low and medium energy collimators for 123I imaging and simultaneous dual-isotope imaging.* Nucl Med Commun, 2003.**

26. **Simon R. Cherry, J.A.S., Michael E. Phelps., *Physics in nuclear medicine*. 3rd ed2003, Philadelphia, PA Saunders.**

27. Barber, C.B., D.P. Dobkin, and H.T. Huhdanpaa, *The Quickhull Algorithm for Convex Hulls.* ACM Transactions on Mathematical Software, 1996. 22(4).

28. Krützmann, N.C., *Application of Complexity Measures to Stratospheric Dynamics.* 2008.

Appendix

Appendix 1

shaking.c

```
#include "udf.h"
    DEFINE_TRANSIENT_PROFILE(movVel,time)
    {
        real vel = 0.0;
        if(time<=0.5)
        {
           vel = 0.3;
        }
    else if(0.5<time&&time<=1.5)
        {
           vel =-0.3;
        }
    else if(1.5<time&&time<=2.5)
        {
           vel = 0.3;
        }
else if(2.5<time&&time<=3.5)
        {
           vel =-0.3;
        }
    else if(3.5<time&&time<=4.5)
        {
           vel = 0.3;
        }
else if(4.5<time&&time<=5.5)
        {
           vel =-0.3;
```

Appendix 2

controlledSpinning.c

```
#include "udf.h"
DEFINE_TRANSIENT_PROFILE(rotation_rate_ramp,time)
{
	real rotation_rate = 0;
	if(time <= 60)
	{
		rotation_rate = 0.5;
	}else
	{
		rotation_rate = 0.0;
	}
	return rotation_rate;
}
```

Appendix 3:

Tc99m_ Co57.m

```
clc;

%-------------------------------------------------------------------------
-----%
% Plot energy spectrum from E.Cam

% Read dicom file
info =
dicominfo('5989228_07165.NM.CRYSTAL_DATA.1000.1.2011.08.11.17.07.15.5
62500.13518958.IMA');

% E.Cam measures photons in 4096 channels
% Create 4096 energy channels in a matrix
energyChannel = (1:1:4096)';

% kev per channel correction factor for detector 1
[x, y] = solve('1015.15*x + y  = 140.5', '892.347*x + y = 122.1');

% Convert energy channels into energies
energy = x*energyChannel+y;

% Load the infomation in CurveData_0
Tc99m_counts = info.CurveData_0;

% Load the infomation in CurveData_0
Co57_counts = info.CurveData_2;

% Normalize the counts by maximum count
Tc99m_normalizedCounts =
double(Tc99m_counts)/max(double(Tc99m_counts));

% Normalize the counts by maximum count
Co57_normalizedCounts = double(Co57_counts)/max(double(Co57_counts));

% Combine energy and normalized counts into a 4096x2 matrix
data1 = [energy Tc99m_normalizedCounts];
data2 = [energy Co57_normalizedCounts];
```

```
subplot(2,1,1);plot(energy,Tc99m_counts,'blue');
hold on
subplot(2,1,1);plot(energy,Co57_counts,'red');

title('The energy spectrum of Tc99m and Co57 from E.CAM measurement')
xlabel('Engery')
ylabel('Counts')
axis tight
hold off
% plot the spectrum of energy vs normalized counts in blue
subplot(2,1,2);plot(energy,Tc99m_normalizedCounts,'blue');
hold on
subplot(2,1,2);plot(energy,Co57_normalizedCounts,'red');
title('The energy spectrum of Tc99m and Co57 in normalized counts from
E.CAM measurement')
xlabel('Engery')
ylabel('Normalised counts')
axis tight
hold off
```

Appendix 4:

EnergyResolutionECAMvsSIMIND.m

```
% Energy resolution validation for E.Cam measurement and Simind simulation
clc;

%-----------------------------------------------------------------%
% Plot energy spectrum from E.Cam

% Read dicom file
info =
dicominfo('5989228_07165.NM.CRYSTAL_DATA.1000.1.2011.08.11.17.07.15.5
62500.13518958.IMA');

% E.Cam measures photons in 4096 channels
% Create 4096 energy channels in a matrix
energyChannel = (1:1:4096)';

% Define energy per channal for Tc99m measurement in detecter 1
energyPerChannal= 0.1384;

% Convert energy channels into energies
energy = energyPerChannal*energyChannel;

% Load the infomation in CurveData_0
counts = info.CurveData_0;

% Normalize the counts by maximum count
normalizedCounts = double(counts)/max(double(counts));

% Combine energy and normalized counts into a 4096x2 matrix
data1 = [energy normalizedCounts];

% plot the spectrum of energy vs normalized counts in blue
plot(energy,normalizedCounts,'blue');
hold on

%-----------------------------------------------------------------
------%
% Plot energy spectrum from simind simulation output
```

```
% Load the data extracted from simind simulation
load('Simind_EnergyResolution.mat');

% The variable in Simind_EnergyResolution.mat is called energyfinal,
% which is a 512x2 matrix. The maximum number of energy channels is 512
in
% simind.
simindData = energyfinal;

% Define energy per channel for simind data
energyPerChannel_sim = 0.352;

% In simind, the energy channel is from 2 to 513, hence, small change has
% to be made before ploting.
simindData = [simindData(:,1)-1  simindData(:,2)];

% Convert energy channels into energies
energy_sim = simindData(:,1)*energyPerChannel_sim;

% In simind, the switch /np was used to produce normalized data.
% The second column of energyfinal is normalized counts, which could
% be used directly.
normalizedCounts_sim = simindData(:,2);

% Final matrix of the simulated data
simindData = [energy_sim,normalizedCounts_sim];

% plot the spectrum of energy vs normalized counts in red
plot(energy_sim,normalizedCounts_sim,'red');

title('The energy spectrum of Tc99m from E.CAM measurement and SIMIND
Simulation')
xlabel('Energy')
ylabel('Normalized counts')
axis tight
hold off
```

Appendix 5:

LineprofileT2.m

```
clear all
close all
clc

% Define ROI parameters
x1 =201;
x2 =300;
y1 =201;
y2 = 300;
% Define the size of line source profile
line_source_profile_size = 5;

% Choose a DICOM file from work folder
[filename, pathname] = uigetfile('*.ima', 'Pick a DICOM  file');
cd(pathname)

% Read the information from detertor 1 and detector2 images
im=dicomread(filename);
im1=im(:,:,1,1);
im2=im(:,:,1,2);

% Extract the data from the defined ROI
ROI1=im1(x1:x2,y1:y2);
ROI2=im2(x1:x2,y1:y2);

% Plot detector1 image with ROI
subplot(3,2,1)
imagesc(im1)
axis  equal tight
title('The detector1 image of IEC line source from E.CAM measurement')
xlabel('x-axis index')
ylabel('y-axis index')
hold on
rectangle('Position',[x1,y1,x2-x1,y2-y1])
colorbar

% Plot detector2 image with ROI
```

```
subplot(3,2,2)
imagesc(im2)
axis  equal tight
title('The detector2 image of IEC line source from E.CAM measurement')
xlabel('x-axis index')
ylabel('y-axis index')
hold on
rectangle('Position',[x1,y1,x2-x1,y2-y1])
colorbar

% Plot detector1 image within the defined ROI
subplot(3,2,3)
imagesc(ROI1)
size_of_image_one = size(im1);
col_of_image_one = size_of_image_one(:,1);
size_of_profile =
round(col_of_image_one/2-line_source_profile_size:col_of_image_one/2+
line_source_profile_size);
axis  equal tight
title('The detector1 image within defined ROI')
xlabel('x-axis index')
ylabel('y-axis index')
colorbar
hold on
x_position = round(col_of_image_one/2-line_source_profile_size)-x1;
rectangle('Position',[x_position,1,line_source_profile_size*2,y2-y1])
;

% Plot the detectcor2 image in the ROI
subplot(3,2,4)
imagesc(ROI2)
axis  equal tight
title('The detector2 image within defined ROI')
xlabel('x-axis index')
ylabel('y-axis index')
colorbar

% Plot the line profile of detector1 image within ROI
subplot(3,2,5)
detector_one_profile = im1(:,size_of_profile);
max_pixel_index =
find(detector_one_profile(:,1)==max(detector_one_profile(:,1)));
```

```
new_index_1 =
-(max_pixel_index-1):1:length(detector_one_profile(:,1))-max_pixel_in
dex;
plot(new_index_1,detector_one_profile(:,1),'r')
title('The detector1 image within defined ROI')
xlabel('Maximum-pixel centred index ')
ylabel('Counts')
hold on

% Mark the pixel index of geometric centre on the profile
geomcent=round(length(detector_one_profile)/2);
plot(geomcent-max_pixel_index,detector_one_profile(geomcent),'*');
axis  tight

% Plot the line spread function of detector1 image within ROI
subplot(3,2,6)
ROI_value = mean(detector_one_profile')';
normalized_ROI_value = ROI_value/max(ROI_value);
row_roi= (1:1:line_source_profile_size*2+1);
max_pixel_index_log = find(ROI_value ==max(ROI_value));
plot(new_index_1,log (normalized_ROI_value) );
title('The line spread function of line source in dectector1')
xlabel('Maximum-pixel centred index ')
ylabel('Normalized Counts')
axis tight
```

Appendix 6:

LineProfileComp.m

```
clear all
close all
clc

% Plot the maximum pixel centred line profile of E.Cam measurement (23cm)
% Define ROI parameters
x1 =206;
x2 =305;
y1 =206;
y2 = 305;

% Define size of region for line profile plotting
line_source_profile_size = 5;

% Choose a DICOM file from experiment

[filename, pathname] = uigetfile('*.ima', 'Pick a DICOM  file');
cd(pathname)

% Read images from e.cam
image = dicomread(filename);

% Read image from detecter 1
image1 = image(:,:,1,1);

% Find the size of image 1
size_of_image_one = size(image1);
% Find the number of column for image 1
col_of_image_one = size_of_image_one(:,1);
% Create the size of the profile from given value
size_of_profile =
round(col_of_image_one/2-line_source_profile_size:col_of_image_one/2+
line_source_profile_size);

% Define the ROI of line profile
detector_one_profile = image1(:,size_of_profile);
% Find the index of  pixel maximum value
```

```
max_pixel_index =
find(detector_one_profile(:,1)==max(detector_one_profile(:,1)));

% Create new index which centred at maximum pixel
new_index_1 =
-(max_pixel_index-1):1:length(detector_one_profile(:,1))-max_pixel_in
dex;

% Taking average values of each pixel from the same row in ROI
ROI_value = mean(detector_one_profile')';
% Normalize the averaged value
normalized_ROI_value = ROI_value/max(ROI_value);

% Plot the line profile in log scale
plot(new_index_1,normalized_ROI_value );

axis tight
hold on

%--------------------------------------------------------------------

% Plot the maximum pixel centred line profile of SIMIND simulation
[filename2, pathname2] = uigetfile('*.h00', 'Pick a interfile');
cd(pathname2)

% Read images from SIMIND file
im_simv=interfileread(filename2);
im_sim = im_simv';
% Find the size of SIMIND image
size_of_image_one_sim = size(im_sim);
% Find the number of SIMIND image
col_of_image_one_sim = size_of_image_one_sim(:,1);
% Create the size of the profile from given value
size_of_profile =
round(col_of_image_one_sim/2-line_source_profile_size:col_of_image_on
e_sim/2+line_source_profile_size);

% Define the ROI of line profile
detector_sim = im_sim(:,size_of_profile);
% Create new index which centred at maximum pixel
max_pixel_index_sim = find(detector_sim(:,1)==max(detector_sim(:,1)));
```

```
new_index_1_sim =
-(max_pixel_index_sim-1):1:length(detector_sim(:,1))-max_pixel_index_
sim;

% Taking average values of each pixel from the same row in ROI
ROI_value_sim = mean(detector_sim')';
% Normalize the averaged value
normalized_ROI_value_sim = ROI_value_sim/max(ROI_value_sim);

% Plot the line profile in log scale
plot(new_index_1_sim,normalized_ROI_value_sim,'r');

title('Line Profile Validation')
xlabel('Maximum-pixel centred index ')
ylabel('Counts')

axis tight
hold off
```

Appendix 7:

LineSpredFunctionComp.m

```
clear all
close all
clc

% Plot the maximum pixel centred line profile of E.Cam measurement(23cm)
% Define ROI parameters
x1 =206;
x2 =305;
y1 =206;
y2 = 305;

% Define size of region for line profile plotting
line_source_profile_size = 5;

% Choose a DICOM file from experiment

[filename, pathname] = uigetfile('*.ima', 'Pick a DICOM  file');
cd(pathname)

% Read images from e.cam
image = dicomread(filename);

% Read image from detecter 1
image1 = image(:,:,1,1);

% Find the size of image 1
size_of_image_one = size(image1);
% Find the number of column for image 1
col_of_image_one = size_of_image_one(:,1);
% Create the size of the profile from given value
size_of_profile =
round(col_of_image_one/2-line_source_profile_size:col_of_image_one/2+
line_source_profile_size);

% Define the ROI of line profile
detector_one_profile = image1(:,size_of_profile);
% Find the index of  pixel maximum value
```

```
max_pixel_index =
find(detector_one_profile(:,1)==max(detector_one_profile(:,1)));

% Create new index which centred at maximum pixel
new_index_1 =
-(max_pixel_index-1):1:length(detector_one_profile(:,1))-max_pixel_in
dex;

% Taking average values of each pixel from the same row in ROI
ROI_value = mean(detector_one_profile')';
% Normalize the averaged value
normalized_ROI_value = ROI_value/max(ROI_value);

% Plot the line spread function from E.Cam
plot(new_index_1,log (normalized_ROI_value) );

axis tight
hold on



%
------------------------------------------------------------------------
-----------------------------------------

% Plot the maximum pixel centred line profile of SIMIND simulation
[filename2, pathname2] = uigetfile('*.h00', 'Pick a interfile');
cd(pathname2)

% Read images from SIMIND file
im_simv=interfileread(filename2);
im_sim = im_simv';
% Find the size of SIMIND image
size_of_image_one_sim = size(im_sim);
% Find the number of SIMIND image
col_of_image_one_sim = size_of_image_one_sim(:,1);
% Create the size of the profile from given value
size_of_profile =
round(col_of_image_one_sim/2-line_source_profile_size:col_of_image_on
e_sim/2+line_source_profile_size);

% Define the ROI of line profile
detector_sim = im_sim(:,size_of_profile);
```

```
% Create new index which centred at maximum pixel
max_pixel_index_sim = find(detector_sim(:,1)==max(detector_sim(:,1)));
new_index_1_sim =
-(max_pixel_index_sim-1):1:length(detector_sim(:,1))-max_pixel_index_
sim;

% Taking average values of each pixel from the same row in ROI
ROI_value_sim = mean(detector_sim')';
% Normalize the averaged value
normalized_ROI_value_sim = ROI_value_sim/max(ROI_value_sim);

% Plot the line spread function from SIMIND
plot(new_index_1,log (normalized_ROI_value_sim),'r');

title('The line spread function validation')
xlabel('Maximum-pixel centred index ')
ylabel('Normalized Counts')
axis tight
hold off
```

Appendix 8:

---------- SIMIND Monte Carlo Program V4.9b----------

INPUT FILE...volumesimula COVER.....al.cr3 SOURCE FILE..smap

OUTPUT FILE..volumesimula CRYSTAL.....nai.cr3 SOURCE MAP...imgvollc.smi

PHANTOM (S)..h2o.cr3 BACK-SCATT...pmt.cr3 DENSITY MAP..

PHANTOM (B)..bone.cr3 SCORE FILE...

---------- FLAGS ----------

Photon Energy	140.50	Matrix		Photons/Proj	604012
Source Type	Integer Maps	Spectra		Activity	500.00
Phantom Type	Hor Cylinder	se-lehr		Detector Radius	29.550
Detector Width	22.250	SPECT		Detector Height	0.952
Upper Window Tresh	151.038	X-Rays		Distance to Det	15.000
Lower Window Tresh	129.962	B-Scatt		X-Shift Source	0.000
Pixel Size (I)	0.695	Random		Y-Shift Source	0.000
Pixel Size (J)	0.695	Cover		Z-Shift Source	0.000
S:Half Length	13.250	Phantom		P:Half Length	13.250
S:Half Width	10.000	Resolut		P:Half Width	10.000
S:Half Height	10.000	Forced		P:Half Height	10.000
Energy Resolution	9.490	IntFile		Max Scatter Ord	3

GENERAL DATA

keV/channel	0.352	Compiler	Windows LF95
Photons/Bq	0.879	Starting Angle	0.000
Camera Offset X	0.000	Cover Thickness	0.100
Camera Offset Y	0.000	Backscatt Thick	0.200
Matrix Size (I)	64	Intrinsic Res	0.360
Matrix Size (J)	64	Acceptance Angle	2.954
Emission Type	2.000	Initial Weight	0.72763E+03
"NN" Scaling Factor	1	Energy Channels	512
Photon Exit Phantom	1	Cutoff energy	0.000

SPECT DATA

Rotation Mode	-360.000	Projections	64.000
Rotation Angle	5.625	Start Projection	1
Orbital Fraction	1.000	End Projection	64

COLLIMATOR DATA FOR CODE: New M Ljungberg

Collimator Code	se-lehr	Collimator Type	Parallel
X:Hole Size	0.111	X:Distance	0.016
Y:Hole Size	0.128	Y:Distance	0.078

X:Center Shift	0.064	Collimator Effic	0.026
Y:Center Shift	0.110	Thickness	2.405
Coll dependent var1	0.000	Coll X-section	pb_sb.cr3
Coll dependent var2	0.000	Hole Shape	Hexagonal
Coll dependent var3	0.000	X-Ray Flag	0
Coll dependent var4	0.000	Movement flag	0.000

Simulation began 2013:07:30 at 15:03:05
Simulation ended 2013:07:30 at 16:06:34
Elapsed time 1 h 3 min and 29 sec
Header file volumesimulation
Image file volumesimulation

INTERACTIONS IN THE CRYSTAL

Detector Hits	754055
Hits/sec	198.8911
Maximum in Spectra	20173.0840
Maximum in Images	867.8015
Count Rate [Total]	33060.7812
Count Rate [Window]	13035.2832

PHOTONS AFTER COLLIMATOR AND WITHIN E-WIN

Geometric	95.77%	93.97%
Penetration	1.88%	4.63%
Scatter in coll	1.02%	1.39%
K-hv	1.33%	0.00%

K-hv1	75.0keV	50.08%	0.00%
K-hv2	72.8keV	28.38%	0.00%
K-hv3	72.1keV	0.05%	0.00%
K-hv4	84.9keV	15.45%	0.00%
K-hv5	87.3keV	6.05%	0.00%

PENETRATED PHOTONS VS. ACCEPTANCE ANGLE (E-WIN)

Angle:	0.3	0.6	0.9	1.2	1.5	1.8	2.1	2.4	2.7	3.0
Pen %:	0.0	0.4	1.7	4.5	10.0	19.1	32.7	51.3	74.6	100.0

RESULTS FROM ENERGY SPECTRUM

Compton Area in Spectrum	0.1260E+07	6.56% (1SD)

Photo	Area in Spectrum	0.8343E+06	1.57% (1SD)
Pileup	Area in Spectrum	0.2136E+05	0.92% (1SD)
Fraction Photo in Window		0.9471	1.36% (1SD)
Fraction Compt in Window		0.0529	6.07% (1SD)

SCATTER RESULTS

Scatter-to-Primary Ratio	0.4099E+00	4.75% (1SD)
Scatter-to-Total Ratio	0.2907E+00	

Scatter in Window by order	1	87.84%
Scatter in Window by order	2	11.33%
Scatter in Window by order	3	0.83%

CALCULATED DETECTOR PARAMETERS

Efficiency	[Peak]	0.3743	1.57% (1SD)
Efficiency	[Detector]	0.9493	
Sensitivity	[cps/MBq]	26.0706	
Sensitivity	[cpm/uCi]	57.8767	
Peak/Compton	[Peak]	29.8725	
Peak/Compton	[Area]	0.6620	
Peak/Total		0.3943	

Inifile: TOMO

Comment: simind.ini

Command: volumesimulation3.smc

Appendix 9

ConvertFluentToSIMIND.m

```
% Convert Fluent Node Data to Volume Source Map for SIMIND Simulation
%
[fileName, pathName] = uigetfile('*.*', 'Select the Fluent file to read');
fullFileName = fullfile(pathName, fileName);  % Generate a full filename
from the parts

rawdata = importdata(char(fullFileName));
data = rawdata.data;

x=data(:,2);
y=data(:,3);
z=data(:,4);
conc = data(:,5);  % concentration

xmin=min(x);
xmax=max(x);
ymin=min(y);
ymax=max(y);
zmin=min(z);
zmax=max(z);

voxels=255;
padding =
min([(xmax-xmin)/voxels,(ymax-ymin)/voxels,(zmax-zmin)/voxels]);

% Some of the following was extracted from
%
http://www.mathworks.com/matlabcentral/fileexchange/1593-genmesh-avs-
to-m
% atlab-converter/content/genmesh.m

%Generate an even grid onto which the actual data will be transposed.
%This even grid is based on the min and max co-ords.
[XI, YI, ZI] =
meshgrid(xmin:padding:xmax,ymin:padding:ymax,zmin:padding:zmax);

%Delaunay transform the dataset (i.e. connect up data points based upon
the selected algorithm)
% doc griddata3 for details of the QuikHull algorithm
```

```
disp('Performing Delaunay tranformation using Griddata3...this may take
quite some time');

GV = griddata3(x,y,z,conc,XI,YI,ZI,'linear');

maxGV = max(GV(:));

% Arbitrary = scale the largest pixel to 30,000 and convert to integers
imgVolume = uint16((30000/maxGV).*GV);

rawslice = squeeze(imgVolume(128,:,:));  % slice through the middle of
the image, squeeze to remove the singleton dimension

imshow(rawslice,[]);  % display the slice

% Write the data to a binary file
% Convert the image data to binary x.y.z image matrix
fid=fopen('imgVolume.smi','wb');  % Write a binary file ready for
importing into SIMIND as a source-matrix.
fwrite(fid, imgVolume,'uint16','l');  % export the whole volume
column-wise as an unsigned integer 16, in little endian byte order ('l')
fclose(fid);  % Close the file
```

Appendix 10:

Reconstruction of the projection data – SIMIND.m

```
% importdata the binary image data - read only and 'little endian' byte
format
% data is float in format of 64x64 prjections (x,y), and 64 of them ('z')
fid = fopen('volumesimulation3.a00', 'r', 'l');  % open a file handle

projectionData =zeros(64,64,64);  % preallocate the image file

% read the image data from the file  - really slow routine. (efficiency
improvement possible)
for k=1:64
    for j=1:64
        for i=1:64
            t(i,j,k)=fread(fid,1,'single','l');
        end
    end
end

% Reconstruct the slices from the projection data generated by SIMIND.
% Reconstruct for a range of positions in the phantom.
theta = 1:5.625:360;  % 64 slices

for j=1:64  % Number of projections

    % extract a set of projections, generating a sinogram image
    sinogram = squeeze(projectionData(:,j,:));  %squeeze is required to
remove the singleton dimension.

    % Reconstruct using the Matlab image processing toolbox iradon (inverse
Radon transform) routine
    % for parallel beam geometry. This is a simple filtered backprojection
routine, except a Hamming filter
    % is uses, and cubic interpolation.
    slices(:,:,z) = iradon(sinogram, theta,'V5cubic','Hamming');  %
cubic interpolation and a Hamming filter
end

% display a series of 8 slices in the central area of the phantom (centred
around the source).
figure;
```

```
offset = 42;
for i = 1:8

    subplot(2,4,i);
    largerImage = imresize(slices(:,:,offset+i),[256 256], 'lanczos3'); %
increase to a smoothed 256x256 image
    imshow(largerImage,[0 150]);  % found this range by inspecting the
data
    title(['Slice ', num2str(offset+i)]);
end

% inverted gray scale
colormap(1-gray);

pause;  % Pause to capture the image

% Display a projection, sinogram, and corresponding reconstructed slice
% Chose slice 47
figure;
subplot(1,3,1);
    imshow(projectionData(:,:,32), []);
    title('Single projection');
subplot(1,3,2);
    imshow(squeeze(projectionData(:,47,:)),[]);
    title('Sinogram for slice 47');
subplot(1,3,3);
    imshow(slices(:,:,47),[]);
    title('Reconstructed slice 47');
colormap(1-gray);
```